

# Weakly supervised training of universal visual concepts for multi-domain semantic segmentation

Petra Bevandić\*, Marin Oršić, Josip Šarić, Ivan Grubišić and Siniša Šegvić

Faculty of Electrical Engineering and Computing, University of Zagreb, Unska 3, Zagreb,  
10000, Zagreb.

\*Corresponding author(s). E-mail(s): [petra.bevandic@fer.hr](mailto:petra.bevandic@fer.hr);

Contributing authors: [marin.orsic@gmail.com](mailto:marin.orsic@gmail.com); [josip.saric@fer.hr](mailto:josip.saric@fer.hr); [ivan.grubisic@fer.hr](mailto:ivan.grubisic@fer.hr);  
[sinisa.segvic@fer.hr](mailto:sinisa.segvic@fer.hr);

## Abstract

Deep supervised models have an unprecedented capacity to absorb large quantities of training data. Hence, training on multiple datasets becomes a method of choice towards strong generalization in usual scenes and graceful performance degradation in edge cases. Unfortunately, popular datasets often have discrepant granularities. For instance, the Cityscapes road class subsumes all driving surfaces, while Vistas defines separate classes for road markings, manholes etc. Furthermore, many datasets have overlapping labels. For instance, pickups are labeled as trucks in VIPER, cars in Vistas, and vans in ADE20k. We address this challenge by considering labels as unions of universal visual concepts. This allows seamless and principled learning on multi-domain dataset collections without requiring any relabeling effort. Our method improves within-dataset and cross-dataset generalization, and provides opportunity to learn visual concepts which are not separately labeled in any of the training datasets. Experiments reveal competitive or state-of-the-art performance on two multi-domain dataset collections and on the WildDash 2 benchmark.

**Keywords:** semantic segmentation, multi-domain training, universal taxonomy

## 1 Introduction

Semantic segmentation has made great progress in recent years across a wide variety of domains [1–4]. The progress is noticeable not only in terms of improved performance on classic datasets [5, 6], but also on recent increasingly complex and challenging benchmarks [7–9]. However, generalization beyond the training domain remains elusive [10]. This suggests that particular datasets introduce unintended pieces of bias that hampers our performance in real-world applications.

Dataset bias can be reduced by training models on multiple datasets [11–13]. This task is straightforward when datasets share the same taxonomy. On the other hand, training on divergent taxonomies such as Cityscapes and Vistas has to be specifically facilitated in some way. One solution is to choose a specific common taxonomy and to impose it to all datasets by relabelling all affected images [10, 12]. If the chosen relabeling policy keeps only the superset classes, the procedure can be carried out automatically. For instance, fine-grained Vistas classes may simply be mapped onto more general Cityscapes classes

[14]. If, however, we wish to keep the fine-grained classes, we must relabel all superclass labels. For instance, all Cityscapes road pixels would have to be disambiguated by hand into some of the Vistas leaf classes. A middle-ground solution alleviates weaknesses of the two extreme approaches by preserving only some fine-grained classes in order to contain the relabeling effort [12].

We address two kinds of inconsistency between taxonomies: discrepant granularity and overlapping classes. Discrepant granularity occurs when a class from dataset A corresponds to several classes from dataset B [15]. For instance the class `road` in Cityscapes is further divided into 8 classes in Vistas: `road`, `bike_lane`, `crosswalk_plain`, `marking_zebra`, `marking_other`, `manhole`, `pothole`, and `service_lane`. Overlapping classes appear when visual concepts get inconsistently grouped across datasets. For instance, pickups are grouped with trucks in VIPER [16], cars and vans in Vistas [7], and vans in ADE20k [17]. We illustrate these two types of labeling inconsistencies in Figure 1.



**Fig. 1:** Common inconsistencies among popular datasets. Images from ADE20k, Viper and Vistas (top) are labeled with discrepant granularity: class `road` from ADE20k and VIPER corresponds to 7 classes in Vistas: `marking-other`, `manhole`, `crosswalk`, `road-other` etc (middle). These datasets have also overlapping labels (bottom): pickups are labeled as `truck` in VIPER, `car` in Vistas, and `van` in ADE20k.

We propose a principled method for training on dataset collections with inconsistent taxonomies. Our method expresses each dataset-specific label as a union of disjunct visual concepts

which we denote as universal classes. For instance, we resolve the problem from the bottom row of Figure 1 by defining universal classes `uni:car`, `uni:van`, `uni:pickup` and `uni:truck`. Figure 2 shows that `VIPER:truck` can be mapped to `uni:truck`  $\cup$  `uni:pickup`, `Vistas:car` to `uni:car`  $\cup$  `uni:van`  $\cup$  `uni:pickup`, and `ADE20k:van` to `uni:van`  $\cup$  `uni:pickup`. Now the posterior probability of each dataset-specific label can be expressed as sum of the corresponding universal posteriors. This allows us to train universal models against particular taxonomies through partial labels [18].

Note that our training setup does not require any relabeling, which means that we do not need to discard any existing classes. Therefore, our universal models capture the full expressiveness of the dataset collection. Our method outperforms all previous baselines, achieves the best overall result on the 2020 Robust Vision Challenge and delivers competitive performance on the WildDash 2 benchmark [19]. We encourage comparison with related and future cross-dataset training approaches by publishing the source code [20] for a universal taxonomy that unifies a collection of ten popular datasets with dense groundtruth.

This paper consolidates our earlier reports [21, 22] and brings several important additions. First, we formalize the necessary conditions for a visual concept to be treated as a learnable universal class. Second, we construct a universal taxonomy that spans 10 datasets from MSeg and RVC collections. Third, we extend a recent mask-level segmentation architecture [4] for multi-dataset learning against our universal taxonomy. The resulting models deliver the first demonstration of universal mask-level prediction in cross-dataset experiments. Finally, we show that knowledge of cross-dataset relations can improve performance even when applied only during inference. This insight can be used as a tool to disambiguate hypotheses about mutually inconsistent class relations during automatic construction of universal taxonomies [23].

Consolidated contributions of our work are as follows. First, we propose a principled procedure for recovering a universal taxonomy for a given dataset collection. Second, we show that our universal taxonomies can be learned by different architectures on original dataset-specific labels according to the logarithm of aggregated

probability (NLL+, NLL max). Finally, our experiments demonstrate that our forms of weak supervision deliver state-of-the-art performance, can learn novel concepts, as well as perform competitively with respect to noiseless learning on opportunistically relabeled data.

## 2 Related work

We consider prior work related to multi-dataset training of semantic segmentation models. We focus on approaches that can learn subclass logits from superclass labels.

### 2.1 Semantic segmentation

Standard semantic segmentation delivers dense categorical predictions [24–27] with respect to the training taxonomy such as PASCAL VOC [6] or Cityscapes [5]. They must retain fine spatial details in order to detect small objects, as well as incorporate a large receptive field in order to disambiguate non-discriminative regions through context [28]. Furthermore, they should be efficient in order to support real-world applications and to preserve environment [29].

Deep convolutional models increase receptive field through subsampling [25, 26]. This strategy also brings improved efficiency and reduced training footprint [2], however a special care is required in order to preserve small objects. Another way to improve context awareness is through pyramidal inputs [3, 30]. Some architectures increase the receptive field or improve efficiency through special kinds of convolutions [31, 32]. Recent approaches trade-off efficiency for improved recognition quality by relying on transformers [4].

Spatial details can be recovered by blending deep layers with the shallow ones [33]. This idea can be carried out throughout an efficient upsampling path with substantially less capacity than the downsampling backbone [14].

Semantic segmentation models have usually been trained as per-pixel classifiers according to the standard cross-entropy loss, which may be inefficient when dealing with a large number of classes. More recent work explores alternative approaches to semantic segmentation. For example, non-parametric models which rely on prototypes and distance-based classification have been shown to work well on large taxonomies

[34]. Improvements have also been achieved by decoupling segment formation from semantic prediction [4, 35]. We demonstrate the flexibility of our universal taxonomies by applying them for cross-dataset training of the Mask2Former architecture.

Recent work shows that single-dataset semantic segmentation may be improved through inclusion of hierarchical information training objectives [37]. Their approach enforces the positive constraints up and negative constraints down the class hierarchy. Similar to their approach, our method enforces positive constraints down the hierarchy tree. Unlike their approach, our method focuses on cross-dataset training with non-leaf labels.

### 2.2 Multi-dataset training

Deep models can absorb huge quantities of labeled data [38]. However, annotated datasets for dense recognition are quite scarce due to being very expensive to procure [39]. Hence, multi-dataset training becomes a prominent avenue towards improved generalization [40]. Multi-dataset training also improves the supervision quality due to discouraging exploitation of dataset bias [10] and facilitating multi-domain inference [12]. Thus, the inclusion of a negative domain into a specialized supervised setup may dramatically improve open-set performance [41–43].

Simple multi-dataset training disregards relations between particular taxonomies by generating predictions with per-dataset heads [11, 44, 45]. These approaches can be useful for pretraining and further finetuning. However, they offer limited value in realistic applications due to being unable to deliver unified predictions. This problem can be addressed by enforcing a consistent common taxonomy through manual relabeling across all datasets [12, 19]. However, manual relabeling is tedious and error-prone. Moreover, future extensions would require further manual relabeling both in existing and the new datasets.

Relabeling can be avoided by detecting relationships between particular taxonomies. Several approaches propose automatic merging of equivalent classes. This can be carried out either through optimization [46], or by merging classes with identical names [12, 13]. However, these approaches are unable to exploit subset/superset relationships. They, therefore, lead to implicit dataset

detection and model overfitting in the presence of overlapping logits.

Very recent work proposes to learn superclass logits on subclass labels in a multi-label segmentation setup [13]. However, their work can not learn universal logits from superset labels. This problem has been addressed by proposing prediction heads with distinct nodes for categories and classes [15, 47]. However, hierarchical taxonomies complicate model training while failing to offer substantial advantages over flat universal taxonomies such as the one proposed in this paper.

## 2.3 Learning with partial labels

Partial labels are a form of weak supervision where a training label corresponds to a set of classes such that only one of the classes is correct. Early work considers the problem of face identification in movie scenes where partial labels can be automatically extracted from screenplays [18]. In this case, a partial label corresponds to the set of all characters present in the scene. In our setup, partial labels are determined by semantic relations between the universal taxonomy and the taxonomies of particular datasets. For example, cars and vans in Cityscapes are labeled with the same class `car`, but our universal taxonomy can discriminate between the two. Hence, we consider the Cityscapes car labels as partial labels corresponding to the set of universal classes `{uni:car, uni:vans}`. The learning objective can be formulated by aggregating predictions that correspond to partial labels. Recent work considers aggregation through sum and max functions but does not find them competitive for object detection [48]. Log-sum-prob loss has been used to alleviate influence of labeling noise at semantic borders [49]. Their method assumes that the pixels are partially labeled with classes found in a  $3 \times 3$  neighborhood.

## 2.4 Learning on pseudo-labels

Pseudo-labeling is a form of semi-supervised learning where a model trained on labeled data provides supervision for unlabeled data [50, 51]. Pseudo-labeling can be viewed as an alternative to weakly supervised learning with respect to a given universal taxonomy. Recent work pseudo-labels object locations in images with the predictions of the heads trained on other datasets [48]. However,

their setup assumes that the label spaces of different datasets do not overlap. Unlike them, we consider semantic segmentation and datasets with overlapping classes.

Very recent work frames universal semantic segmentation as a regression problem towards pseudo-labels provided by a pre-trained language model [52]. However, label semantics may vary across datasets. Indeed, another recent work finds that visual cues give rise to better cross-dataset semantic relations than language-based representations [53]. Another recent work recovers complex subset/superset relations that would be difficult to find with language embeddings [23].

# 3 Method

This section describes our approach for multi-dataset training of universal visual concepts. We introduce universal models, propose a procedure for constructing a universal taxonomy over a given dataset collection, formulate a suitable weakly supervised objective, implement our method within the mask-level context, and discuss removal of untrainable classes. Most of our considerations are applicable in any categorical recognition context. Still, we focus on dense prediction where our method has most practical value due to huge cost of ground-truth annotations.

## 3.1 Terminology and notation

We use the following terminology and notations:

- we typeset dataset-specific classes in typewriter font as `Dataset:class`; we abbreviate Cityscapes as `City` and WildDash2 as `WD`;
- we consider a semantic class  $c$  as a set of all image pixels that should be annotated as  $c$ ;
- we express semantic relationships according to set notation, e.g.: `Vistas:sky = City:sky`, `City:road  $\supset$  Vistas:manhole`, `VIPER:truck  $\cap$  Vistas:car = WD:pickup`, `City:road  $\perp$  City:car  $\iff$  City:road  $\cap$  City:car =  $\emptyset$` ;
- a taxonomy  $\mathcal{S}$  is a set of mutually disjoint semantic classes:  $\forall c_i, c_j \in \mathcal{S}: c_i \perp c_j$ ;
- a universal taxonomy  $\mathcal{U}$  encompasses the entire semantic range of the considered dataset collection:  $\bigcup_{u \in \mathcal{U}} u = \bigcup_d \mathcal{S}_d$ ; each universal class can intersect at most one class from each dataset:  $\forall u \in \mathcal{U}, c \in \bigcup_d \mathcal{S}_d: (u \perp c) \vee (u \subseteq c)$ ;

- a union of taxonomies is a pseudo-taxonomy if its members have non-empty intersections:  $\mathcal{S}_{VIPER} \cup \mathcal{S}_{Vistas}$  is a pseudo-taxonomy since  $VIPER:truck \not\subseteq Vistas:car$  (cf. Fig. 1);
- a semantic segmentation dataset  $\mathcal{D}_d$  consists of images and corresponding dense labels:  $\mathcal{D}_d = \{(\mathbf{x}^d, \mathbf{y}^d)\}$ ; the labels correspond to semantic classes  $c \in \mathcal{S}_d$ , where  $\mathcal{S}_d$  is the taxonomy of the dataset  $\mathcal{D}_d$ .

### 3.2 Universal models

We consider training a flat universal model on multiple datasets with incompatible labeling policies. Our universal taxonomies ensure that each dataset-specific class can be mapped to a union of disjoint universal classes as illustrated in Figure 2.

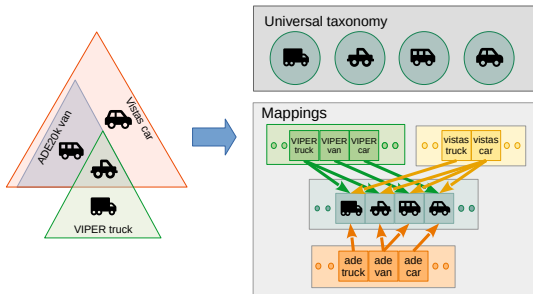


**Fig. 2:** We address the semantic overlaps from the bottom row of Fig. 1 by mapping each label (left) to a set of disjoint universal classes (right). Our universal taxonomy spans the entire semantic range of the considered dataset collection.

Universal models output a distribution over fine-grained universal classes that amalgamate semantic knowledge of all training datasets. They are therefore very convenient for practical applications in the wild where we desire graceful performance degradation in presence of anomalies and hard edge cases. Furthermore, each dataset-specific posterior can be recovered as a sum of corresponding universal posteriors. Thus, universal models can be trained by leveraging dataset-specific ground truth as partial labels [18]. Finally, they can be evaluated on dataset-specific test data. These three ways to interact with a universal model are illustrated in Figure 3.

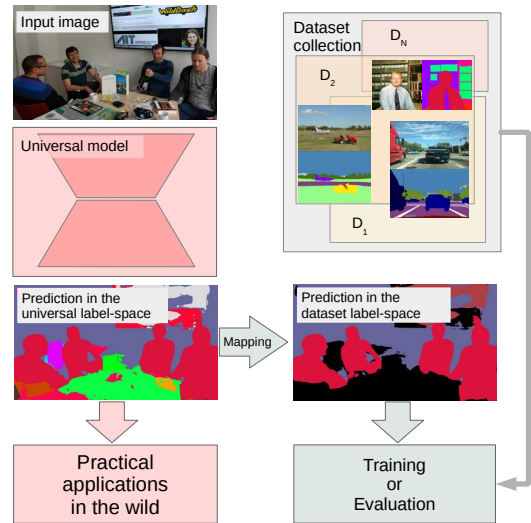


**Fig. 3:** Our models allow universal inference in the wild (left) as well as multi-dataset training and validation on dataset-specific labels (right).

### 3.3 Creating a universal taxonomy

We propose a principled procedure for recovering the universal taxonomy for a given collection of datasets. Figure 4 shows that we start the process with the multiset  $\mathcal{M}$  that contains each class from all dataset-specific taxonomies. We iteratively transform  $\mathcal{M}$  according to rules that resolve three types of overlaps between classes. Concurrently we update the mappings that connect dataset-specific classes to the remaining classes in  $\mathcal{M}$ . Initial mappings are identity functions. The three rules for overlap resolution can be formulated as follows.

1. If two classes  $c_i$  and  $c_j$  match exactly, then we replace them with a new class  $c'$  and remap both  $c_i$  and  $c_j$  to  $c'$ .  
*Example:* Since  $WD:sky$  and  $City:sky$  are equivalent, we merge them into  $M:sky$ , and define mappings:  $WD:sky \mapsto M:sky$ ,  $City:sky \mapsto M:sky$ .
2. If a class  $c_i$  is a superset of a class  $c_j$ , then  $c_i$  is removed from  $\mathcal{M}$ , a new class  $c'_i = c_i \setminus c_j$  is added, while  $c_i$  is remapped to  $\{c_j, c'_i\}$ .  
*Example:*  $KITTI:car$  is a superset of  $ADE20k:car$  because it contains vans. We therefore add classes  $M:van$  and  $M:car$ , and create mappings  $KITTI:car \mapsto \{M:car, M:van\}$  and  $ADE20k:car \mapsto \{M:car\}$ .

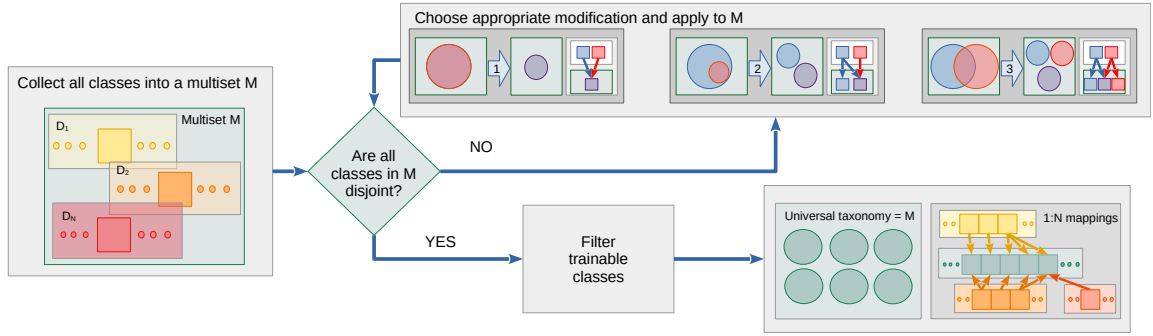


**Fig. 4:** Construction of a universal taxonomy. We collect all dataset-specific classes into the multiset  $\mathcal{M}$  (left). Then, we iteratively modify  $\mathcal{M}$  according to the three resolution rules from section 3.3 (top-right). The iteration continues until all classes in  $\mathcal{M}$  are disjoint (center). Finally, we filter universal classes that can not be trained with the available supervision (bottom-right).

3. If two classes overlap,  $(c_i \not\perp c_j) \wedge (c_i \setminus c_j \neq \emptyset) \wedge (c_j \setminus c_i \neq \emptyset)$ , then  $c_i$  and  $c_j$  are replaced with three new disjoint classes  $c'_i = c_i \setminus c_j$ ,  $c'_j = c_j \setminus c_i$ , and  $c' = c_i \cap c_j$ . Class  $c_i$  is remapped to  $\{c'_i, c'\}$ , while  $c_j$  is remapped to  $\{c'_j, c'\}$ .

*Example:* VIPER:truck contains trucks and pickups while ADE20k:truck contains trucks and trailers. We therefore replace VIPER:truck and ADE20k:truck with M:truck, M:pickup and M:trailer, and create the following mappings: VIPER:truck  $\mapsto$  {M:truck, M:pickup} and ADE20k:truck  $\mapsto$  {M:truck, M:trailer}.

The process ends when all rules are no longer applicable. At this moment, all remaining classes within  $\mathcal{M}$  are disjoint. Furthermore, they have equal or finer granularity than all dataset-specific classes. In other words, each dataset-specific class maps to a subset of classes from  $\mathcal{M}$ . Consequently,  $\mathcal{M}$  now corresponds to a taxonomy that encompasses the entire semantic range of the considered dataset collection.

### 3.4 NLL+ loss

We model the probability of universal classes as per-pixel softmax over universal logits  $\mathbf{s}$ . Let the random variable  $U$  correspond to a universal prediction at a particular pixel, and let  $\mathbf{p}$  denote the softmax output. Then, the posterior probability of a single universal class  $u$  corresponds to:

$$P(U = u | \mathbf{x}) = \text{softmax}(\mathbf{s}_u). \quad (1)$$

Let the random variable  $Y$  denote a dataset-specific prediction at a particular pixel and let  $m_{\mathcal{S}_d} : \mathcal{S}_d \rightarrow 2^U$  denote our mapping from dataset-specific classes to subsets of universal classes. Then, we can express the posterior of a dataset-specific class  $y$  as a sum of the posteriors of universal classes  $u' \in m_{\mathcal{S}_d}(y)$  in the same pixel:

$$P(Y = y | \mathbf{x}) = \sum_{u' \in m_{\mathcal{S}_d}(y)} P(U = u' | \mathbf{x}). \quad (2)$$

If we substitute that sum into the standard negative log likelihood for that pixel, then we obtain negative log-likelihood over aggregated universal posteriors, which we denote as NLL+:

$$\begin{aligned} \mathcal{L}^{\text{NLL}+}(\mathbf{x}, y | m_{\mathcal{S}_d}) &= -\ln P(Y = y | \mathbf{x}) \\ &= -\ln \sum_{u' \in m_{\mathcal{S}_d}(y)} P(U = u' | \mathbf{x}). \end{aligned} \quad (3)$$

NLL+ loss exploits weak supervision by learning fine-grained logits on coarse-grained labels of particular datasets. Experiments will show that such loss can learn visual concepts that are not explicitly labeled in any of the datasets.

To better understand training with the NLL+ loss, it is helpful to analyze its partial derivatives with respect to universal logits  $\mathbf{s}$ . We start by expressing the NLL+ loss in terms of the logits:

$$\begin{aligned} \mathcal{L}^{\text{NLL}+}(\mathbf{x}, y | m_{\mathcal{S}_d}) &= \\ &= -\ln \sum_{u' \in m_{\mathcal{S}_d}(y)} P(U = u' | \mathbf{x}) \end{aligned}$$

$$\begin{aligned}
&= -\ln \frac{\sum_{u' \in m_{s_d}(y)} \exp s_{u'}}{\sum_{u \in \mathcal{U}} \exp s_u} \\
&= \ln \sum_{u \in \mathcal{U}} \exp s_u - \ln \sum_{u' \in m_{s_d}(y)} \exp s_{u'}. \quad (4)
\end{aligned}$$

From this we get the following gradients of the loss with respect to the universal logit  $s_v$ :

$$\begin{aligned}
\frac{\partial \mathcal{L}}{\partial s_v} &= \frac{\partial}{\partial s_v} \ln \sum_{u \in \mathcal{U}} \exp s_u - \frac{\partial}{\partial s_v} \ln \sum_{u' \in m_{s_d}(y)} \exp s_{u'} \\
&= \frac{\exp s_v}{\sum_{u \in \mathcal{U}} \exp s_u} - \frac{\mathbb{1}[v \in m_{s_d}(y)] \exp s_v}{\sum_{u' \in m_{s_d}(y)} \exp s_{u'}} \\
&= P(U = v | \mathbf{x}) - P(U = v | Y = y, \mathbf{x}). \quad (5)
\end{aligned}$$

If  $v$  is not associated with the label  $y$ , then the gradient is strictly positive and exactly the same as in the standard case with crisp labels. The NLL+ loss pushes incorrect logits to  $-\infty$  just the same as the standard NLL.

If  $v$  is a subset of  $y$ , then the gradient is strictly negative since  $P(U = v | \mathbf{x}) \leq P(U = v | y, \mathbf{x})$ . Furthermore, the magnitude of the gradient will be proportional to  $P(U = v | Y = y, \mathbf{x})$ . Thus, the gradients favour the universal class that is currently winning, and that class will become even more probable after the update. If the model succeeds to lock onto the correct universal class, then the gradient of the correct logit will be the same as in the standard supervised case.

### 3.5 Mask-level recognition

This section applies universal taxonomies for multi-dataset training of recent semantic segmentation models based on mask-level recognition. We consider a simplified version of a recent architecture that can be described as Mask2Former with fixed matching [4, 35]. Figure 5 shows that the considered architecture consists of a down-sampling backbone, pixel decoder and transformer decoder. The pixel decoder upsamples the backbone features towards per-pixel embeddings  $E \times H \times W$ . The transformer decoder produces the matrix  $E \times U$  that projects embeddings onto universal multi-label logits. Finally, the logits give rise to universal semantic maps through independent sigmoid activation.

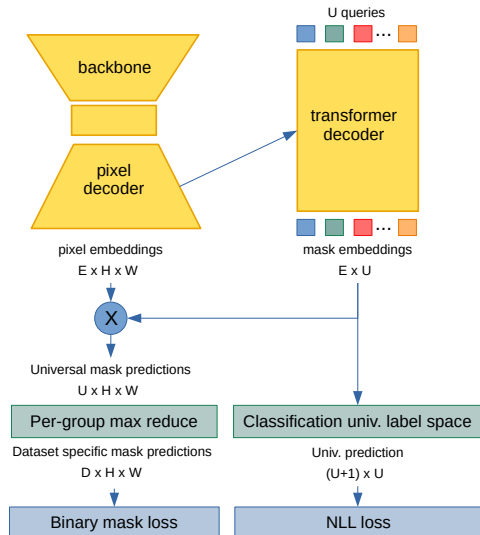


**Fig. 5:** We propose an extension of the M2F architecture with fixed matching that can be trained with our universal taxonomy. The model assigns pixels to universal classes according to sigmoid-activated dot products between mask embeddings and pixel-level embeddings. We recover dataset-specific masks as maximum pixel-level assignments over the associated universal classes (6).

The  $U$  vectors of the projection matrix are classified into  $U$  universal classes and one null class. The resulting categorical distributions are required to match the corresponding universal classes through standard NLL loss so that each embedding corresponds to a single universal class. The binary mask predictions are trained through combination of dice and focal loss.

Note that we can not score universal masks through NLL+ due to sigmoid activation. Instead, we propose to perform the aggregation through the max function:

$$m_y[i, j] = \max_{u \in m_{s_d}(y)} m_u[i, j]. \quad (6)$$

### 3.6 Determining trainable logits

Learning with partial labels can never learn a universal class which is always labeled together with some other universal class. More formally, a universal class  $u$  is not learnable if there is another universal class  $u'$  that is a subset all

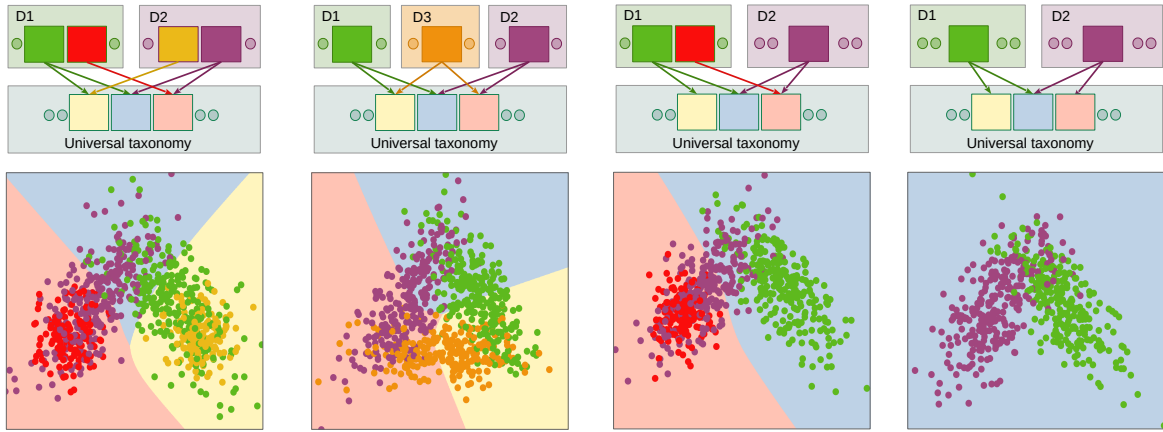


**Fig. 6:** Some universal taxonomies can not be learned with NLL+. The top row shows dataset-specific taxonomies and their mappings to the universal taxonomy. The bottom row shows the training samples (coloured points) and the learned decision landscape (coloured regions). NLL+ succeeds to learn concepts at intersections of dataset-specific classes (columns 1 and 2). However, if a tuple of universal classes is always labeled as the same superset class, NLL+ learns to predict only one of them (columns 3 and 4).

dataset-specific classes that  $u$  is a subset of:

$$\exists u' \in \mathcal{U}, \forall c \in \bigcup_d \mathcal{S}_d, (u \subset c \Rightarrow u' \subset c). \quad (7)$$

In such cases, no training label prefers classification into  $u$  instead of into  $c \setminus u$ . Hence, there is no advantage to assign a nontrivial probability to  $u$ .

We illustrate this failure mode with an example that corresponds to the rightmost toy problem in Fig. 6. Classes from the example will correspond to colours from the toy problem. Suppose we wished to recognize universal classes `uni:rider` (blue), `uni:pedestrian` (yellow) and `uni:bicycle` (pink) by NLL+ learning from labels `CamVid:bicycle` (violet) = `uni:bicycle`  $\cup$  `uni:rider` and `Pascal:person` (green) = `uni:rider`  $\cup$  `uni:pedestrian`. Unfortunately, this setup will simply learn to predict both `camvid:bicycle` and `pascal:person` as `uni:rider` since such solution perfectly minimizes the loss. Although, there are some good solutions that could recognize `uni:bicycle` and `uni:pedestrian`, the NLL+ loss provides no incentive to find them since the optimisation problem is underconstrained. On the other hand, if we introduced labels that map to `uni:bicycle` and `uni:pedestrian` independently from `uni:rider`, the optimization would learn all three universal

classes. This behaviour is a common limitation of all forms of learning with partial labels [18].

Figure 6 demonstrates the ability of the NLL+ loss to learn separate concepts from overlapping labels on four toy problems over 2D data. Each label from row 1 is mapped to universal classes in row 2. We annotate the training samples with the label colors, and the decision surfaces with the colours of the universal classes. The two rightmost toy problems show that some universal logits may die off due to insufficient supervision. On the other hand, the two leftmost columns show that NLL+ optimization succeeds whenever the partial labels provide enough learning signal. These two toy problems also show that NLL+ can learn to recognize universal concepts that are never labeled as a standalone class.

There is no need to keep universal classes which would die off during training since that would only reduce the model efficiency. Following this realization, we introduce another processing step to our procedure for recovering the universal taxonomy (cf. Figure 4). The new processing step filters universal classes that have no chance to succeed during training due to always co-occurring with at least one of the siblings.



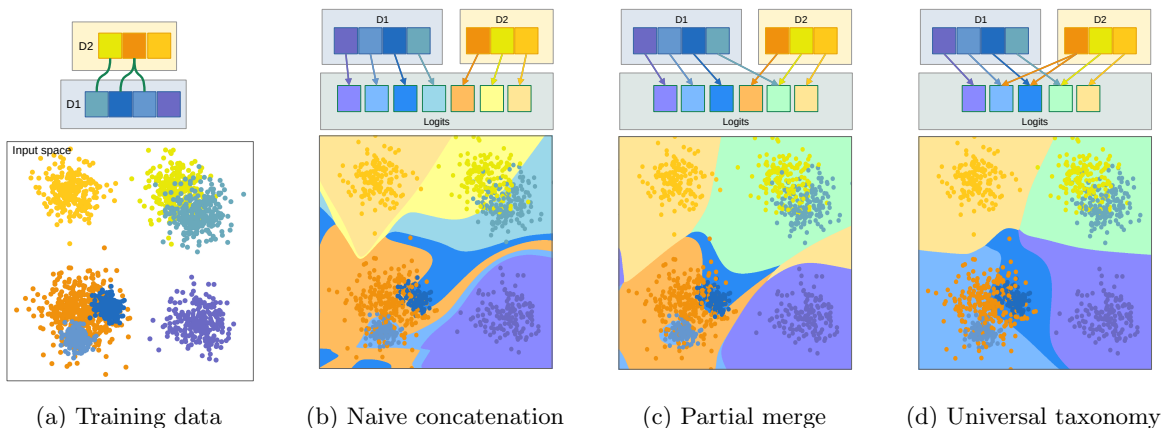


**Fig. 7:** Multi-dataset training on two toy datasets with semantically related classes (a). Our models (b-d) involve shared features and flat softmax predictions. Naive concatenation is unaware of all semantic relations (b). Partial merge is aware of class equivalence (c). Our universal model is aware both of class equivalence and class overlap (d). The two baselines (b-c) learn ragged decision boundaries due to conflicting gradients in overlapping classes. Smooth decision landscape of the universal model (d) suggests that avoiding competition between semantically related concepts improves generalization.

## 4 Experimental setup

Our experiments validate the proposed method against several baselines and compare it against the previous work. Our baselines involve strongly supervised learning on two pseudo-taxonomies and universal learning with pseudo-relabeled ground truth. We take special care in order to properly evaluate predictions that fall outside of the particular evaluation taxonomy. Our experiments promote fair comparison by pairing approaches with the same architecture. We carefully describe the implementation details in order to promote reproducibility of our experiments.

### 4.1 Baselines

Multi-dataset training can be conceived by complementing shared features with per-dataset segmentation heads [11, 45]. However, realistic applications require inference in mixed-content images. For instance, an autonomous vehicle should be able to recognize a COCO chair on a Vistas road. This requirement could be addressed by supplying an additional head for dense dataset recognition. In this case, we can recover the joint posterior of class  $c$  and dataset  $\mathcal{D}$  in each pixel according to:

$$P(c, \mathcal{D} | \mathbf{x}) = P(c | \mathcal{D}, \mathbf{x}) \cdot P(\mathcal{D} | \mathbf{x}) \quad (8)$$

However, dataset recognition does not make much sense when training on datasets from the same domain (e.g. Vistas and WildDash 2). Moreover, submissions with explicit dataset recognition have been outright prohibited at major multi-domain recognition competitions [40]. Hence, we consider another two baselines that outperform per-dataset heads in our multi-dataset experiments.

We now consider a related alternative approach that we denote as naive concatenation. Similarly to per-dataset heads, the naive concatenation also assigns a distinct training logit to each dataset-specific class. The only difference is that here all logits get jointly activated with a common softmax. Such models have to discriminate semantically related classes from different datasets, or, in other words, perform a kind of implicit dataset recognition. This promotes overfitting to dataset bias instead of encouraging cross-dataset generalization. For instance, we can not hope to learn anything useful from discriminating Vistas cars and WildDash cars. Besides wasting the model capacity on dataset recognition, redundant logits hamper the training due to increased memory footprint. Furthermore, the inferred semantics has to be post-processed if we wish to consolidate related logits from different taxonomies.

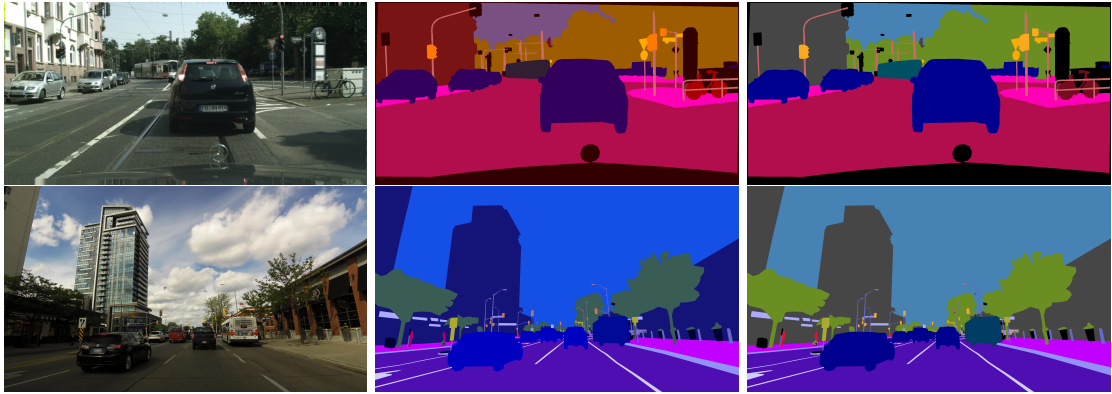


**Fig. 8:** We illustrate the training logits for our two baselines and joint training on Cityscapes and Vistas. The rows show validation images from the two datasets. The columns show the input image, the naive concatenation ground truth, and the partial merge ground truth. In naive concatenation all classes are considered semantically separate. In partial merge identical classes such as sky, vegetation and building are merged into the same class, while overlapping classes such as road and road marking remain separate.

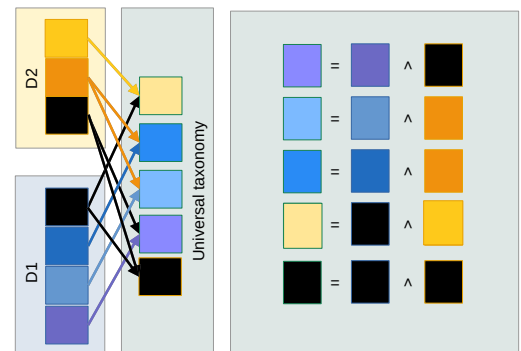
Drawbacks of naive concatenation can be mitigated by merging classes with identical semantics. We refer to the resulting approach as partial merge, since it is unable to consolidate overlapping classes. In comparison with naive concatenation, this approach reduces the waste of capacity but it does not completely eliminate the competition between related logits. For instance, a partial merge model would have independent logits for `WD:road` and `Vistas:crosswalk`. Such model would need to discriminate WildDash crosswalks from Vistas crosswalks, and that does not encourage generalization in the wild. We conclude that partial merge models still have to discriminate datasets, and that this problem can be addressed only through a proper universal taxonomy.

Figure 7 compares naive concatenation and partial merge with our universal approach on a toy 2D problem. Dataset  $\mathcal{D}_1$  consists of 4 classes that we designate with blue hues. Dataset  $\mathcal{D}_2$  consists of 3 classes that we designated with yellow hues. Subfigure (a) shows that there is one 1:1 correspondence and one 2:1 correspondence between classes of  $\mathcal{D}_1$  and  $\mathcal{D}_2$ . Thus, naive concatenation has 7 logits, partial merge has 6 logits, while our universal taxonomy has 5 logits. We observe that our universal model is likely to generalize better due to smoother decision surfaces.

Figure 8 compares the training taxonomies of naive concatenation and partial merge for joint training on Cityscapes and Vistas.

## 4.2 Universal pseudo-labels

Training with the NLL+ loss (3) introduces some noise into the learning process, since the model may overfit to any of the incorrect universal classes of the partial label. This noise can be removed by manually refining the labels towards correct universal classes. However, manual relabeling is slow and costly. Hence, we consider to collect universal pseudo-labels by considering predictions trained on particular datasets.



**Fig. 9:** Universal classes may be defined as unique tuples of dataset-specific classes. Therefore, an ensemble of dataset-specific open-set classifiers can deliver universal pseudo-labels.

We start by noting that each universal class can be expressed as intersection of the associated

dataset-specific classes. Thus, we may represent each universal class with a unique set of labels. Consider the taxonomy from Figure 2. Class `uni:pickup` could be defined as `VIPER:truck`  $\cap$  `Vistas:car`  $\cap$  `ADE20k:van`, while `uni:van` could be defined as `VIPER:van`  $\cap$  `Vistas:car`  $\cap$  `ADE20k:van`. Note that some universal classes can be orthogonal with respect to a given dataset. For example, `uni:cushion` would be defined as `ADE20k:cushion`, since cushions are outliers for VIPER and Vistas datasets. This suggests that closed-set classifiers are not suitable for universal pseudo-labeling as they produce false positives in outlier pixels.

Consequently, we consider open-set dataset-specific taxonomies that introduce a separate class for the unknown visual world. In this case, `uni:cushion` would be defined as `ADE20k:cushion`  $\wedge$  `VIPER:outlier`  $\wedge$  `Vistas:outlier`. Consequently, one could perform such pseudo-labelling with ensembles of dataset-specific models as shown in Figure 9.

However, the quality of pseudo-labels could be further improved by leveraging the ground truth. Suppose we are given an input image and the corresponding dense labels  $(\mathbf{x}^a, \mathbf{y}^a) \in \mathcal{D}_a$ . Then we can express dense pseudo-labels for a universal class  $u$  as sum of conditional per-dataset scores:

$$\mathbf{S}(u | \mathbf{x}^a, \mathbf{y}^a) = \sum_{d \neq a} \mathbf{S}^d(u | \mathbf{x}^a, \mathbf{y}^a). \quad (9)$$

We formulate  $\mathbf{S}^d$  in terms of predictive probabilities of a model trained on  $\mathcal{D}_d$ . The score depends on whether  $\mathcal{D}_d$  contains a class  $c_i^d \in \mathcal{S}_{\mathcal{D}_d}$  that maps to the universal class  $u$  ( $c_i^d \mapsto u$ ). Note that there can be at most one such class since we assume that all datasets have proper taxonomies. If  $c_i^d$  does not exist or if the ground truth  $\mathbf{y}^a$  in the particular pixel  $(r, k)$  does not map to  $u$ , then  $S_{rk}^d(u | \mathbf{x}^a, y_{rk}^a) = 0$ . Otherwise, the score approximates the conditional probability of  $c_i^d$  given the ground truth  $y_{rk}^a$ :

$$S_{rk}^d(u | \mathbf{x}^a, y_{rk}^a) = \frac{\mathbb{P}(Y_{rk} = c_i^d | \mathbf{x}^a)}{\sum_{c_j^d \neq y_{rk}^a} \mathbb{P}(Y_{rk} = c_j^d | \mathbf{x}^a)} \quad (10)$$

Assume we wish to pseudo-relabel a pixel labeled as `Vistas:car` according to a model trained on VIPER. Figure 2 shows that the candidate universal classes are `uni:pickup`, `uni:van` and `uni:`

`car`. We observe that the knowledge of the correct Vistas class limits the possible VIPER predictions to `VIPER:truck`, `VIPER:van` and `VIPER:car`. We therefore recover the desired pseudo-label by only looking at these three VIPER classes. For example, the score  $S^{\text{VIPER}}(\text{uni} : \text{pickup} | \mathbf{x}, \text{Vistas} : \text{car})$  would be determined by dividing the posterior of `VIPER:truck`, with the sum of posteriors for the three VIPER classes that intersect the ground truth. We illustrate the pseudo-labeling based on dataset-specific ground-truth in Figure 11.

Finally, we recover pseudo-labels by applying  $\arg \max$  over ensembled scores (9) of all universal classes that relate to the ground truth. This allows to train universal models through the standard NLL-loss with respect to the pseudo-labels. Note that this approach faces the following two shortcomings: i) two-step training, and ii) pseudo-labels could be inaccurate due to domain shift. We compare pseudo-reabeled universal models with our weakly supervised models in section 5.

### 4.3 Evaluation of foreign predictions

Universal models are not easily evaluated since the ground truth is almost never expressed in the universal domain. We therefore evaluate our universal models by converting our universal predictions to dataset-specific taxonomies according to Equation (2). This conversion may get complicated, since some universal logits may not correspond to any class of the considered evaluation dataset. We shall refer to such universal logits as foreign or extra-distribution logits.

We propose to deal with this issue by extending each dataset-specific taxonomy with a special void class that maps to all universal classes that are foreign to this particular taxonomy. Note that such practice is compatible with major multi-domain recognition competitions, since they explicitly allow post-processing of universal predictions before submissions to individual benchmarks [40]. We determine the posterior of the void class according to the equation (2), just the same as we would do for any regular class. Many semantic segmentation benchmarks accept void predictions and penalize them less strictly than incorrect within-domain predictions. More precisely, void predictions increase only the count of false negatives while not affecting the count of false positives for a given ground-truth class.

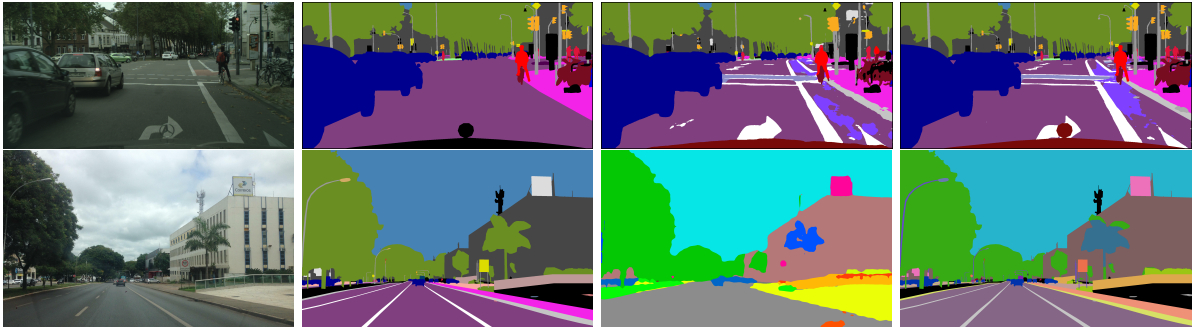


**Fig. 10:** We form universal pseudo-labels by refining native labels according to predictions from foreign dataset-specific models. The two rows illustrate pseudo-labels Cityscapes  $\rightarrow$  Cityscapes-Vistas, and Vistas  $\rightarrow$  ADE20K-Vistas. The columns show: the input image, native ground-truth, foreign predictions and our universal pseudo-labels. Note that the prediction mistakes from column 3 are reduced in column 4. This is evident on edges of cars and distant poles (top), and the palm trunk (bottom).

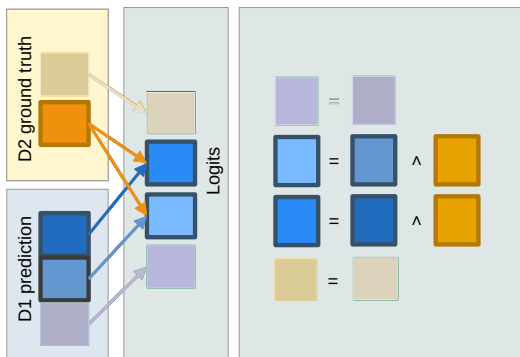


**Fig. 11:** Universal pseudo-labels can be constructed by refining native ground-truth according to dataset-specific predictions. This improves the quality of pseudo-labels due to fewer conflicts with respect to a pure prediction-based approach (cf. Fig. 9 and Fig. 10).

We adopt the same convention in our validation experiments.

#### 4.4 Post-inference mapping

Different from universal models, the baseline approaches may deliver foreign predictions even in cases of good recognition. For instance, a naive concatenation model often recognizes COCO:sky as Vistas:sky. Partial merge models experience similar failure modes, although less often. We see that the baselines could improve through post-inference agreement with semantic relations. We therefore propose to score each evaluation class  $c_i^a$  by summing its posterior with posteriors of all

intersecting foreign classes  $c_j^b$ :

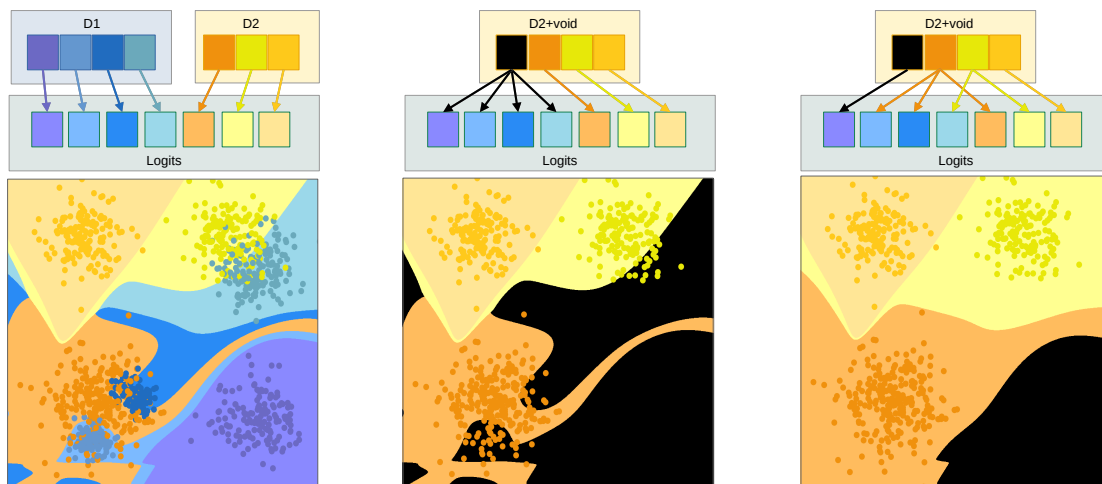
$$\mathbf{S}(c_i^a | \mathbf{x}^a) = \mathbf{P}(c_i^a | \mathbf{x}^a) + \sum_{c_j^b \neq c_i^a} \mathbf{P}(c_j^b | \mathbf{x}^a). \quad (11)$$

Figure 12 evaluates naive concatenation according to post-inference mapping (11) on the same toy problem as in Figure 7, and compares it to default scoring. We observe that post-inference mapping leads to smoother decision surfaces that promise better generalization.

#### 4.5 Implementation details

Our semantic segmentation experiments reduce the computational complexity of multi-domain training by leveraging pyramidal SwiftNet models [3]. Small experiments from 5.1 and 5.4 involve a ResNet-18 [54] backbone. Large experiments on multi-dataset collections from 5.3, 5.5 and 5.6 involve a checkpointed DenseNet-161 backbone [14, 55]. We denote these two models as Snp-RN18 and Snp-DN161. All our M2F experiments use the ResNet-18 backbone.

We train our universal models according to NLL+ loss (3). All other approaches use the standard NLL loss. Both losses prioritize pixels at semantic borders [56]. We use the Adam optimizer and attenuate the learning rate with cosine annealing from  $5 \cdot 10^{-4}$  to  $6 \cdot 10^{-6}$ . Our submissions to the RVC 2020 benchmark collection [40] were trained for a fixed number of epochs. All other experiments train only on the training splits of the involved datasets and use early stopping with



(a) naive concatenation (all classes)      (b) default scoring (D2)      (c) post-inference mapping (D2)

**Fig. 12:** We train the naive concatenation model for the same toy problem as in Figure 7 (a), and subsequently evaluate on D2 (b-c). Default scoring assigns all foreign logits to the void class and thus triggers many undesired void predictions that we show in black (b). A large proportion of these void predictions swings to the correct class when we score with post-inference resolution (c) according to (11).

respect to the average validation mIoU. Please note that our validation experiments on WildDash 2 split the training images and labels into minitrain and minival according to the alphabetical ordering. We place first 572 images into minival and the remaining images into minitrain.

We augment training images with horizontal flipping, random scaling between  $0.5\times$  to  $2\times$  and random cropping. We use  $768\times 768$  crops except when training on the MSeg dataset collection where we use  $512\times 512$  crops. In experiments on ADE20k, Vistas as well as MSeg and RVC collections, we start augmentation by upsampling images so that the smaller side is 1080 pixels. We apply the same preprocessing to the test images as well and proceed by downsampling predictions to the input resolution. Most of our experiments use a single Tesla V100 32 GB and set the common batch size with respect to the most memory inefficient model. Our RVC submissions have been trained and evaluated on 6 such GPUs. Our minibatches prefer images with multiple class instances and rare classes, as well as encourage even representation of datasets.

## 5 Results

We validate our universal taxonomies by comparing them against the three baselines in 5.1, and training on relabeled data in 5.3. We demonstrate that NLL+ loss can learn unlabeled visual concepts in 5.4. We evaluate our universal models on the RVC benchmark collections in 5.5, and on the WildDash 2 benchmark in 5.6.

### 5.1 Baselines

We consider joint training on three pairs of datasets: i) Vistas - Cityscapes, ii) Vistas - WildDash 2 (WD2) and iii) Vistas - ADE20k. In the first setup, all Vistas classes are either equivalent or subsets of their Cityscapes counterparts. Hence, the universal taxonomy coincides with the Vistas taxonomy. The second setup also pairs two road-driving datasets, however here both datasets are quite diverse. Consequently, we expect more competition between related logits from the two taxonomies. The third setup pairs datasets from different domains. The training batch sizes are 18 for road-driving setups and 10 for Vistas-ADE20k.

Table 1 compares our weakly supervised universal approach (universal - NLL+) with the three

Taxonomy	post-inference mapping	(Vistas-City)		(Vistas-WD2)		(Vistas-ADE20k)	
		City	Vistas	WD2	Vistas	ADE20k	Vistas
single dataset	N/A	76.7	46.4	50.6	46.4	35.7	46.4
per-dataset heads	no	77.1	43.3	55.0	42.2	36.5	39.3
per-dataset heads	(11)	76.9	43.4	54.7	42.5	36.6	40.1
naive concat	no	76.8	44.4	54.8	42.8	36.8	41.0
naive concat	(11)	76.8	44.4	55.3	43.1	36.8	42.2
M2F naive concat	no	78.5	52.8	60.3	51.5	N/A	N/A
M2F naive concat	(11)	78.5	52.8	61.1	51.5	N/A	N/A
partial merge	no	77.1	44.5	54.5	44.0	37.3	41.1
partial merge	(11)	77.1	44.5	54.7	44.1	37.4	41.8
universal - pseudo	(2)	76.9	44.9	55.5	45.5	34.1	43.7
universal - NLL+	(2)	77.0	44.9	56.2	44.4	37.4	42.8
M2F universal	(6)	77.4	52.9	60.5	52.1	N/A	N/A

**Table 1:** Evaluation of joint training on Vistas-City, Vistas-WD2, and Vistas-ADE20k (mIoU). Post-inference mapping contributes noticeable improvement where dataset detection is difficult (Vistas-WD2, Vistas-ADE20k). Leveraging our universal taxonomy in different setups outperforms the baselines. Weakly supervised learning with NLL+ generalizes slightly better than two-step learning on pseudo-relabeled data in spite of much simpler training.

baselines and training on pseudo-labels according to (9). All approaches map foreign logits to the void class, as explained in section 4.3. The baseline with per-dataset heads [11, 45] determines the joint posterior of classes and datasets according to (8). We observe that partial merge outperforms naive concatenation, and that naive concatenation outperforms independent per-dataset heads. Overall, all baselines profit from post-inference mapping (11), although we notice most improvement on Vistas-WD2 and Vistas-ADE20k.

The table indicates that our universal approaches outperform single-dataset training on all datasets except Vistas. This suggests that dense prediction on Cityscapes, WD2 and ADE20k can succeed by trading off capacity for additional supervision. Furthermore, our universal approaches outperform per-dataset heads, naive concatenation, and partial merge. The advantage is least evident in the Cityscapes-Vistas experiment. This effect is likely due to all Cityscapes images being acquired with the same camera and in similar environment and weather. This uniformity enables easy dataset detection and alleviates contention across related classes. The table

also indicates that NLL+ succeeds to match and marginally outperform two-step training with universal pseudo-labels. The advantage is especially prominent in the case of Vistas-ADE20k, which is likely due to the large domain shift between the two taxonomies. We note that pseudo-relabeling would perform much worse without having access to our universal taxonomy, and that it would likely improve if pseudo labels were provided by our universal model.

Tables 2 and 3 validate road-driving models from Table 1 on road-driving datasets that were not seen during training: CamVid (CV) [57], KITTI (KIT) [58], BDD [59] and IDD [60]. All baseline models were evaluated with post-inference mapping. All models map foreign predictions to class void. This comparison assesses quality of the learnt features, and generalization potential of different approaches.

Our universal approaches either outperform the baselines or are within the variance. Weak supervision with NLL+ is consistently slightly better than two-step learning on pseudo-relabeled data. The contribution of our approach is somewhat more prominent in the Vistas-WD setup

Model	WD2	CV	KIT	BDD	IDD
single dataset	50.6	73.9	N/A	58.7	59.5
per-dataset	42.8	74.4	55.3	58.0	41.6
naive concat	43.3	74.1	58.9	56.7	42.4
partial merge	43.8	73.9	59.4	57.0	43.0
univ - pseudo	42.4	73.3	58.1	57.5	42.6
univ - NLL+	<b>43.9</b>	<b>75.3</b>	<b>60.5</b>	<b>58.0</b>	<b>42.8</b>

**Table 2:** Cross-dataset evaluation of joint training on Vistas-City (mIoU). We evaluate models from Table 1 on WildDash 2 mini val, CamVid test, KITTI val, BDD val, and IDD val.

Model	City	CV	KIT	BDD	IDD
single dataset	76.7	73.9	N/A	58.7	59.5
per-dataset	69.3	72.8	52.6	58.1	41.5
naive concat	69.0	72.7	<b>53.6</b>	56.1	41.6
partial merge	69.8	72.4	53.5	57.1	41.9
univ - pseudo	71.2	74.5	52.6	<b>59.2</b>	42.4
univ - NLL+	<b>71.4</b>	<b>74.9</b>	53.0	59.0	<b>42.6</b>

**Table 3:** Cross-dataset evaluation of joint training on Vistas-WD2 (mIoU). We evaluate models from Table 1 on Cityscapes val, CamVid test, KITTI val, BDD val, and IDD val.

where there is more competition between semantically related logits. Note that KITTI performance heavily depends on whether Cityscapes images were seen during training. This is most likely due to significant similarity between the two datasets.

## 5.2 Mask-level recognition

Table 4 considers a Mask2Former architecture that was adapted for multi-dataset training according to Fig. 5. We jointly train the proposed model on Vistas and Cityscapes, and present its performance along the NLL+ model from Table 1. Note that the two models are not comparable since the transformer decoder has much more parameters than ResNet-18.

We observe that, qualitatively, our universal M2F model behaves similarly to our pixel-based models in previous experiments. Notably, within-domain performance suffers only a minor performance hit with respect to single-dataset experiments (0.2 pp on Cityscapes, 1.2 pp on Vistas). As expected, cross-dataset performance exhibits sensitivity to domain shift, which is best observed on

Model	within		cross-dataset				
	City	Vistas	WD2	CV	KITTI	BDD	IDD
univ-NLL+	77.0	44.9	43.9	75.3	60.5	58.0	42.8
univ-M2F	77.4	52.9	49.8	79.4	72.3	61.4	50.3

**Table 4:** Multi-dataset training of a mask-level model (M2F) for semantic segmentation. The M2F model succeeds to learn a universal taxonomy and to deliver prominent cross-dataset generalization.

the IDD dataset. Nevertheless, our method succeeds to deliver reliable universal predictions after learning on dataset-specific labels.

## 5.3 MSeg collection

We consider a large-scale collection of the following seven datasets: ADE20k [17], BDD [59], Cityscapes [5], COCO [8], IDD [60], SUN RGBD [61] and Vistas [7]. This collection is of particular interest because it has been manually relabeled towards a custom taxonomy known as MSeg. The MSeg taxonomy has 194 classes that are consistently labeled across all seven datasets [12]. However, in order to contain the manual relabeling effort, the MSeg taxonomy drops 61 dataset-specific classes. Pixels with these labels either get relabeled to a superset class (e.g. `COCO:floor-wood` is replaced with `MSeg:floor`) or outright ignored (e.g. `Vistas:catch-basin`).

We construct our universal taxonomy for the MSeg collection according to the procedure from section 3.3. Our taxonomy consists of 255 universal classes that allow unambiguous prediction of all dataset-specific classes in the entire collection. We train our universal model on original labels of the seven datasets according to NLL+ loss and compare it with standard learning on MSeg labels.

Please note that models trained on MSeg labels are not in the same ballpark with our universal models who get to see only original labels. Still, the comparison provides some insight into the trade-off between flexibility of weak supervision and noiseless learning on opportunistically relabeled data. We train all models on a single Tesla V100 for 20 epochs with batch size 10. We consider two evaluation protocols since the MSeg taxonomy is not able to recognize all evaluation classes from the seven datasets. The MSeg protocol only considers the 194 classes that are retained

Eval. protocol	Taxonomy	ADE20k	BDD	City	COCO	IDD	SUN	Vistas
Default	MSeg	28.4	<b>61.9</b>	<b>77.0</b>	34.3	47.4	<b>47.3</b>	28.7
	universal - NLL+	<b>35.6</b>	60.4	76.1	<b>39.3</b>	<b>56.7</b>	46.9	<b>44.2</b>
MSeg	MSeg	38.5	<b>61.9</b>	<b>77.0</b>	<b>40.9</b>	<b>61.9</b>	<b>47.3</b>	47.6
	universal - NLL+	<b>39.7</b>	60.4	76.1	40.3	58.1	46.9	<b>49.9</b>

**Table 5:** Multi-domain experiments with SNp-DN161 on the seven MSeg datasets. We compare standard learning on relabeled data (MSeg) with weakly supervised learning on original labels (Universal - NLL+), according to two evaluation protocols (Default, MSeg). The models are evaluated on validation subsets of the seven datasets by mapping all foreign predictions to class void.

in the MSeg taxonomy [12], while the default protocol considers all classes from the particular datasets. Note that experimental performance on Cityscapes, BDD and SUN RGBD will not depend on the chosen protocol since the MSeg taxonomy incorporates all classes from these three datasets.

Table 5 summarizes performance metrics of the two models according to the two protocols. Our approach slightly underperforms on the three datasets that are fully preserved within the MSeg taxonomy. This can be attributed either to noisy NLL+ training or to depleted model capacity due to learning 61 more classes. Top section of the table presents evaluation according to the default protocol. Our approach prevails by a wide margin (from 5 to 16 percentage points) on all four datasets that are not fully represented by the MSeg taxonomy. Bottom section of the table presents evaluation according to the MSeg protocol. Somewhat surprisingly, our approach remains competitive in spite of inferior supervision, especially on the three datasets with the largest individual taxonomies - ADE20k (150), COCO (133), and Vistas (65). Differences across the two dataset groups could be due to our training procedure allocating more model capacity to datasets with more rare classes. This hypothesis is based

on observation that dropped classes are comparatively rare. Overall, the table seems to suggest that harnessing flexibility of weakly supervised universal taxonomies may be more cost-effective than strengthening supervision by manual relabeling, especially when considering options for including future datasets. Figure 13 presents a qualitative comparison of different models trained on the MSeg collection.

Table 6 studies the frequency of void predictions for several models trained on the MSeg dataset collection. We observe that our universal approach and the MSeg approach tend to produce less void predictions than the two baselines. The naive concatenation model performs the worst, while the model with partially merged classes sits somewhere in-between. This suggests that foreign predictions are related to the competition between related visual concepts from different datasets.

The presented experiments also show that the amount of void predictions is not uniform across datasets. This indicates that some of the datasets are easy to detect due to uniform image acquisition (camera, weather, location etc.). Furthermore, batch creation and dataset sizes might introduce various kinds of bias into the models. In the end, no approach is uniformly better or

Taxonomy	mapping	ADE20k	BDD	Cityscapes	COCO	IDD	SUN	Vistas
naive concat	no	1.9	1.2	0.0	6.7	0.1	1.4	0.2
partial merge	no	0.8	0.5	0.0	2.3	0.9	0.2	0.0
MSeg	no	0.6	0.2	0.0	0.3	0.5	0.3	0.5
universal - NLL+	(2)	0.2	0.3	0.0	0.7	0.3	0.1	0.1

**Table 6:** Percentage of foreign predictions in multi-domain experiments with SNp-DN161 on the seven MSeg datasets according to the default protocol. We conjecture correlation between foreign predictions and competition between overlapping classes. The overall incidence of wrong predictions is around 15%.



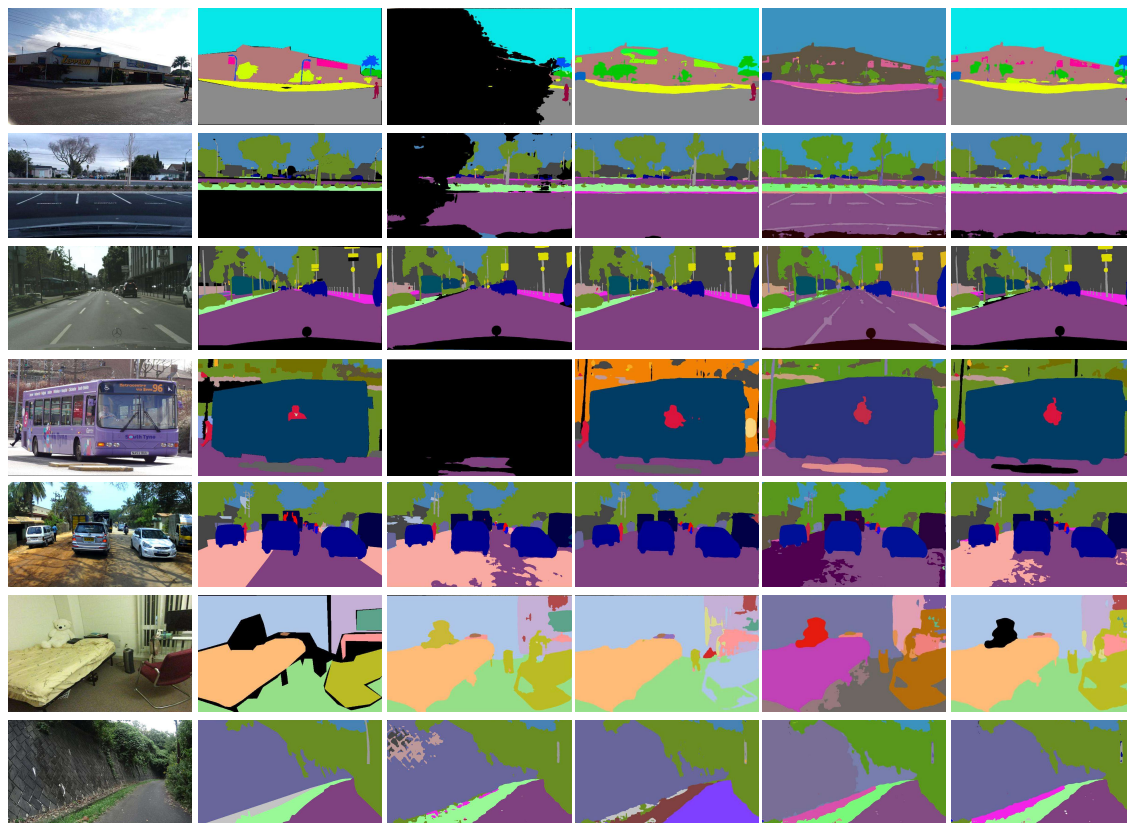


**Fig. 13:** Qualitative evaluation of multi-domain models on MSeg images (top to bottom): ADE20K, BDD, Cityscapes, COCO, IDD, SUN RGBD, and Vistas. The columns present the input image (column i), ground-truth labels (ii), as well as predictions of naive concatenation (iii), the MSeg model (iv), and our model in universal (v) and native dataset-specific labels (vi). Naive concatenation triggers void predictions (black) in contested classes. This is especially common in images from diverse datasets (ADE20k, BDD, COCO). The MSeg model cannot recognize some dataset-specific classes such as palm tree (ADE20k), tree (COCO) and parking lot (IDD). Our model recognizes universal classes and connects them with their dataset-specific counterparts such as marking-other  $\rightarrow$  road (BDD, Cityscapes) or curb  $\rightarrow$  sidewalk (ADE20k, Cityscapes). Multi-dataset training enables outlier detection in dataset-specific predictions (teddy bear, SUN RGBD).

worse on all datasets. Furthermore, limitations of dataset-specific evaluation can favour overfitting to specific scenery (e.g. KITTI) or noisy labels (e.g. BDD). These challenges could be addressed by collecting novel test images and annotating them with ground-truth labels from several dataset-specific taxonomies. Such evaluation would compel the models to recognize visual concepts in unusual surroundings and thus bring us closer to universal computer vision.

## 5.4 Novel concepts

The toy example in Figure 6 suggests that NLL+ should be able to learn novel concepts that are not explicitly labeled in any of the datasets. We test this hypothesis by splitting Cityscapes train and relabeling the two subsets with overlapping taxonomies according to Figure 14. The two subsets have approximately equal size and class distribution. The subset "City-4wheel" includes images from cities between Aachen and Hanover, and groups trucks, buses and cars into

the class `four-wheels-vehicle`. The subset "City-personal" includes the remaining images and groups cars, bicycles and motorcycles into the class `personal-vehicle`. Both subsets have 17 classes. Note that cars are never labeled as a standalone class, whereas buses, trucks, motorcycles and bicycles occur as standalone classes in only one of the two splits.

In this setup, the universal taxonomy consists of the standard 19 classes of the Cityscapes dataset as shown in Figure 14. Each standalone class is mapped to itself. The two composite classes are mapped as follows: `four-wheel-vehicle`  $\mapsto$  `uni:car`  $\cup$  `uni:bus`  $\cup$  `uni:truck`, and `personal-vehicle`  $\mapsto$  `uni:car`  $\cup$  `uni:bicycle`  $\cup$  `uni:motorcycle`.

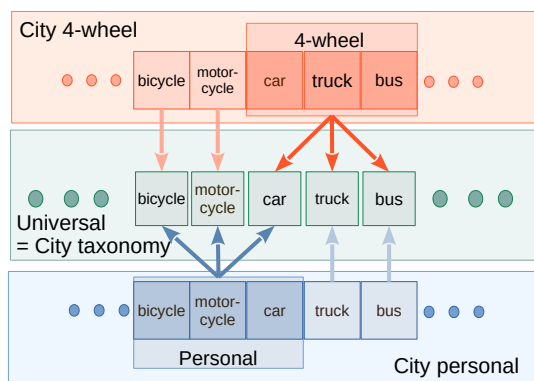


**Fig. 14:** We relabel Cityscapes train into two subsets. Subset "City 4-wheel" groups cars, buses and trucks. Subset "City personal" groups cars, bicycles and motorcycles. Universal taxonomy for the two splits includes all 19 Cityscapes classes.

We validate our method (NLL+) against four other multi-dataset approaches. The NLL baseline simply ignores all composite labels and therefore should not be able to recognize the class `car`. Naive concatenation and partial merge are the two baselines from section 4.1. NLL-max is a modification of our approach that replaces the summation in (2) with the probability of the most likely universal class. We also include the model trained on the standard Cityscapes train dataset, and denote it as oracle since it receives more supervision than the other approaches. The oracle exposes the handicap due to weak supervision and shows the upper bound of multi-dataset training. We

train all models for 250 epochs with batch size 14 on a single GTX1080 by oversampling images with instances of class `train`.

Model						mIoU
NLL baseline	0	54.2	43.9	32.5	60.3	58.7
NLL-max	0	9.6	40.8	1.6	75.7	61.8
naive concat	91.1	61.4	42.2	39.0	72.3	67.6
partial merge	92.4	54.3	55.1	39.0	74.3	71.4
NLL+	<b>93.6</b>	<b>73.3</b>	<b>66.6</b>	<b>46.4</b>	75.4	<b>74.3</b>
M2F concat	92.9	53.1	60.7	35.4	76.7	72.5
M2F universal	95.1	77.7	75.4	54.7	77.6	77.7
NLL oracle	94.4	82.9	72.9	62.2	76.5	76.2
M2F oracle	95.3	84.2	76.5	61.0	78.8	77.6

**Table 7:** Experimental validation of multi-dataset training on relabeled Cityscapes according to the setup from Figure 14. NLL baseline ignores all composite labels, while NLL oracle trains on original Cityscapes labels in all images. Our universal taxonomy becomes even more advantageous in M2F experiments where it performs au pair with the oracle.

Table 7 shows that NLL-max delivers poor performance and that it can not detect cars. A closer look revealed that NLL-max is prone to overfitting to universal classes that receive direct supervision through the other dataset. More concretely, 46% of training pixels at cars were recognized as buses while the rest were recognized as motorcycles. Note that this effect can not arise in setups without overlapping classes [48]. The two baselines succeeded to recognize cars due to post-inference mapping (11), however they underperform with respect to NLL+. We attribute the success of our method to learning with partial labels, as well as to principled formulation of the weakly supervised objective. We observe most improvement on classes with only half standalone labels (`bus`, `truck`, `motorcycle`, `bicycle`). These improvements arise due to contribution of learning with partial labels, and absence of competition between related logits. This competition is especially influential in this particular setup since there is very little domain shift between the two training splits.

Qualitative experiments from Figure 15 demonstrate the ability of our universal models to learn novel concepts in ADE20K and COCO.

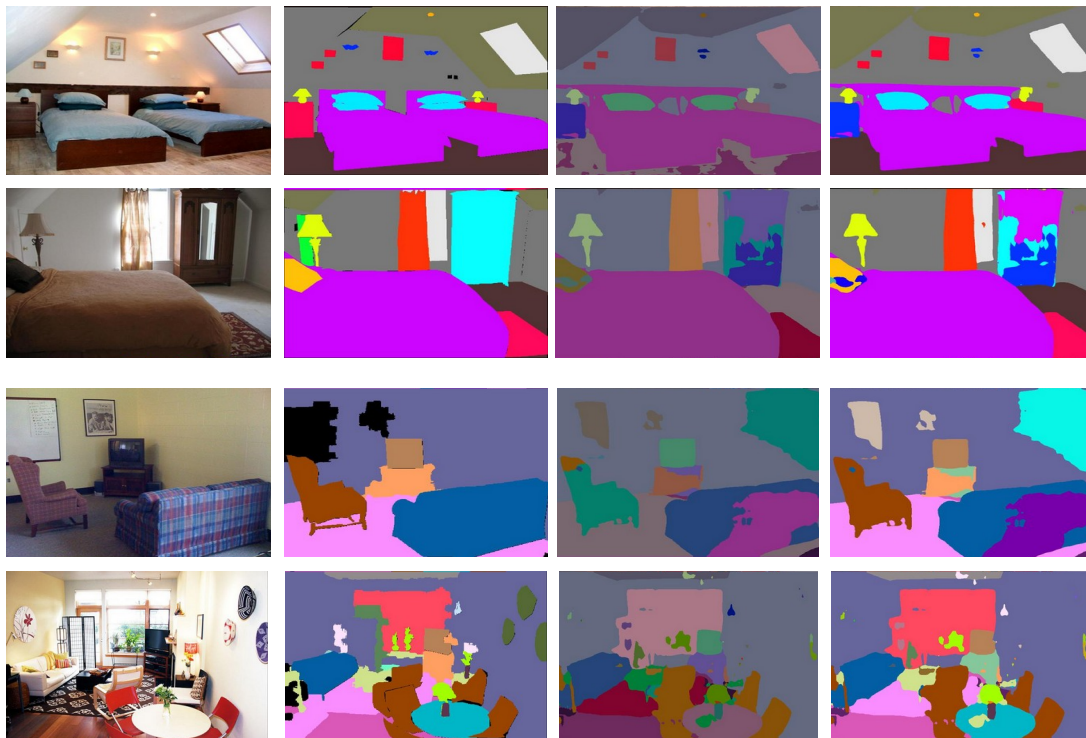


**Fig. 15:** We demonstrate the ability of our universal models to learn novel concepts on ADE20K (top two images) and COCO (bottom two images). The columns show the input image, the dataset-specific ground truths, the universal predictions and the dataset-specific prediction. Both ADE20K and COCO contain classes `floor` (dark brown in ADE20K, dark purple in COCO) and `carpet` (red in ADE20k, pink in COCO). The difference between the two datasets is that ADE labels carpeted floors with the class `floor` (dark brown, row 2) while COCO labels carpeted floors with the class `carpet` (pink, row 3). Our universal taxonomy contains classes `uni:floor` (purple), `uni:carpeted floor` (gray) and `uni:carpet` (dark red). The mappings are:  $\text{ADE20k-floor} \mapsto \text{uni:floor} \cup \text{uni:carpeted floor}$ ,  $\text{ADE20k-carpet} \mapsto \text{uni:carpet}$ ,  $\text{COCO-floor} \mapsto \text{uni:floor}$ , and  $\text{COCO-carpet} \mapsto \text{uni:carpet} \cup \text{uni:carpeted floor}$ . Using our approach, we are able to train the model to recognize carpeted floors as a standalone visual concept that can be connected to the correct dataset-specific class.

## 5.5 RVC challenge

Robust Vision Challenge is a prominent recent competition in multi-domain computer vision [40]. The challenge promotes real-world usability by requiring the submitted models to perform well on multiple benchmarks akin to combined events in athletics. The challenge considers several tasks in dense reconstruction and recognition, however here we consider only the semantic segmentation track that requires submissions to ADE20k, Cityscapes, KITTI [58] (only in 2020), Vistas, Scannet [62], Viper [16] and WildDash 2 [10].

RVC submission rules aim to reward cross-domain competence and to discourage brute-force solutions that thrive by overfitting to dataset bias. Thus, all benchmark submissions have to be inferred by a single model with less than 300 training logits. The predictions must reside in a universal label space that is dataset-agnostic. In other words, explicit dataset recognition and dataset-specific sub-solutions are outright prohibited. These requirements disqualify naive concatenation and per-dataset heads. Note that the universal predictions have to be projected to the particular dataset-specific taxonomy for each

benchmark submission. This can be implemented by multiplying universal predictions with a matrix whose rows correspond to dataset-specific classes.

The challenge allows training on any publicly available data. Still we choose to train only on the seven training subsets due to overwhelming computational complexity. Table 8 presents the basic RVC training setup that involves quarter trillion labeled pixels, 35× more than in Cityscapes.

Dataset	content	images	classes	$\sqrt{\text{pixels}}$
ADE20k	photos	22210	150 - 150	460±154
City	driving	3475	28 - 19	1448±0
KITTI	driving	200	28 - 19	682±1
VIPER	GTA-V	18326	32 - 19	1440±0
ScanNet	interior	24902	40 - 20	1109±78
Vistas	driving	20000	65 - 65	2908±608
WD2	driving	4256	26 - 20	1440±0

**Table 8:** Basic RVC training setup. The columns show the number of annotated non-test images, the number of training and test classes, as well as mean and standard deviation of the square root of the number of pixels ( $\sqrt{HW}$ ) across images.

We construct the universal taxonomy for the basic RVC collection according to the procedure from section 3.3. Our source code for mapping each dataset-specific class to the corresponding subset of 192 universal classes is available online [20]. There is one case where we stray from our procedure in order to prevent proliferation of twin classes. Vistas, KITTI and Cityscapes label vehicle windows as vehicles, while VIPER labels those pixels with what is seen through the glass. Consistent application of rule 3 would require forking each VIPER class (e.g `person-through-glass` or `vegetation-through-glass`). Instead, we introduce simplifying assumptions such as `VIPER:car = Vistas:car` and `Vistas:car ⊥ VIPER:person` in order to reduce the footprint of the universal models.

We increase the model capacity by setting the upsampling width to 384 channels. We leverage checkpointed backbones [2, 63] and custom backprop through NLL+ loss in order to allow training on batches of  $8 \times 768^2$  crops per 32GB GPU. We perform the training on 6 V100 32 GB GPUs for 100 epochs. We minimize boundary modulation [56] on ScanNet images in order to alleviate noisy labels. The total complexity of our training setup is around 4 exaFLOP or four days on our hardware. Our benchmark submissions are ensembled

predictions on original images and their horizontal reflections across six scales. Inference took one day on our hardware.

Model	ADE	City	KIT	MV	SN	VIP	WD
MSeg [12]	<b>33.2</b>	<b>80.7</b>	62.6	34.2	48.5	40.7	35.2
SNp_rn152	31.1	74.7	63.9	40.4	<b>54.6</b>	62.5	45.4
SNp_dn161f	30.8	77.9	<b>68.9</b>	<b>44.6</b>	<b>53.9</b>	<b>64.6</b>	<b>46.8</b>

**Table 9:** Performance evaluation on the RVC 2020 semantic segmentation track. We submit the same model to the seven benchmarks: ADE20k (ADE), Cityscapes (City), KITTI (KIT), Vistas (MV), ScanNet (SN), VIPER (VIP) and WildDash 2 (WD). The model from the bottom section has been submitted after the challenge deadline.

Table 9 presents performance evaluation on RVC 2020. The top section shows the two valid submissions to RVC 2020 semantic segmentation track [40]. Our submission outperforms the model trained on the MSeg taxonomy [12] due to being able to recognize all classes from the particular benchmarks. Our approach succeeded due to being able to adapt to the task at hand without requiring any manual relabeling. The bottom section shows our improved model that was trained as explained in the previous paragraphs. We show it separately because it was submitted to the seven benchmarks after the deadline for RVC 2020.

The winners of the RVC 2022 semantic segmentation track [67] use a taxonomy obtained by the partial merge approach. Our experiments are not directly comparable with that work since their computing budget is 10 times larger than ours (64 GPUs vs 6 GPUs). This makes a large difference in speed of training as well as in available model capacity since they can train on batches of 1 crop per GPU. The runners-up of the RVC 2022 semantic segmentation track [68] construct their universal taxonomy according to an early account of our procedure from the section 3.3 [21]. Their method showcases a great generalization performance in spite of being trained on modest hardware (4 V100 GPU). In comparison with our RVC 2020 model, our submission to RVC 2022 featured a more ambitious training setup (we included BDD and COCO to the training collection) and a stronger backbone (ConvNeXt Large).

Yet, the performance was only slightly better than at RVC 2020. Post-challenge validation has shown that ladder-style upsampling [3] is not an effective design for large taxonomies.

## 5.6 WildDash 2

Multi-domain training discourages overfitting to dataset bias and anticipates occurrence of outliers during inference. This makes it a prominent approach towards robust performance in the real world. We explore this idea in more depth by analyzing the performance of our RVC model on the WildDash 2 benchmark.

The WildDash dataset collects challenging road-driving imagery from across the whole world. This sounds similar to Vistas but there is one important difference. Instead of aiming at a typical distribution of world-wide road-driving scenes, WildDash aims at edge cases that are likely to break image understanding algorithms. Just as Vistas is a step up from Cityscapes, so WildDash further raises the bar in several important aspects.

Wilddash is the first dataset to specifically target expected points of failure of dense prediction models. It explicitly enumerates visual hazards such as underexposure, motion blur or particles [10], and quantifies their impact to the prediction quality. Furthermore, it includes a negative test dataset from various non-driving contexts that contains semantic anomalies with respect to typical road-driving taxonomies. In all pixels of

negative test images, the model is allowed to predict either a void prediction or a best-case ground truth. Thus, WildDash could be seen as a precursor to recent dataset for open-set segmentation and dense anomaly detection [69, 70].

Table 10 presents the actual WildDash2 leaderboard. Our RVC 2022 model achieves the best classic segmentation score and a slightly better robustness to common hazards. We achieve a slightly lower overall score due to worse performance on negative images. Available qualitative results [40] suggest that we find more positive content in negative images than the competing approaches.

Figure 16 shows qualitative performance of our model on negative images. Columns show (left to right): the input image, the prediction in the universal taxonomy, and the prediction in the WildDash 2 taxonomy. We designate void pixels with black colour. The negative images were taken in non-road driving contexts (rows 1-4) or from an unusual perspective (row 5). These images may contain pixels which conform to WildDash semantics such as people or walls (row 2). Correct predictions of these pixels are counted as true positives.

## 5.7 Discussion

This work, proposes manual universal taxonomies for encoding visual relations between classes in different datasets. Our approach encourages knowledge exchange between datasets during either

Model	Meta Avg mIoU cla	Classic				Negative mIoU cla	Hazards avg. impact
		mIoU cla	iIoU cla	mIoU cat	iIoU cat		
EffPS_b1bs4sem_RVC [64]	32.2	35.7	24.4	63.8	56.0	20.4	-8%
MSeg_1080 [12]	35.2	38.7	35.4	65.1	50.7	24.7	-12%
seamseg_rvcsubset [65]	37.9	41.2	37.2	63.1	58.1	30.5	-13%
UniSeg [13]	39.4	41.7	35.3	65.8	57.4	34.8	-13%
FAN_NV_RVC [67]	47.5	50.8	44.0	<b>74.2</b>	67.5	34.4	-8%
MIX6D_RVC [68]	<b>48.5</b>	51.2	<b>46.5</b>	72.4	66.1	<b>40.8</b>	-8%
SNp_RN152pyr_RVC [21]	45.4	48.9	42.7	70.1	64.8	32.5	-7%
SN_DN161_fat_pyrx8 [22]	46.8	51.0	43.9	71.4	65.5	32.6	-8%
UNIV_CNP_RVC_UE	46.9	<b>51.6</b>	45.9	72.8	67.5	29.0	<b>-6%</b>

**Table 10:** Current WildDash 2 leaderboard. All submissions have been trained on multiple datasets. The bottom section presents our RVC models. The first two entries correspond to our models from Table 9 (we had to shorten them there in order to fit the tight layout). We also include two unpublished submissions to RVC 2022 (FAN\_NV, MIX6D). FAN\_NV was trained with 10× hardware with respect to our models.

training or inference. The proposed NLL+ loss includes this knowledge into standard multi-class training, and has the ability to transfer information down the label hierarchy. We note that our framework is applicable to different kinds of architectures. For example, prototype-based approaches could have prototypes for universal classes, which could be associated with their dataset-specific counterparts. We demonstrate the flexibility of our universal taxonomies by applying them for multi-class training of the recent M2F architecture.

Our concurrent work [23] shows that it is possible to automate universal taxonomy construction. Still, we consider manual universal taxonomies as a useful baseline for measuring progress of the automatic methods. Furthermore, manual universal taxonomies present an opportunity to evaluate other computer vision tasks. For example, a concurrent work on automatic discovery of visual relations between datasets [53] performs experiments on the MSeg taxonomy that omits 61 classes and thus cannot properly encode all possible class

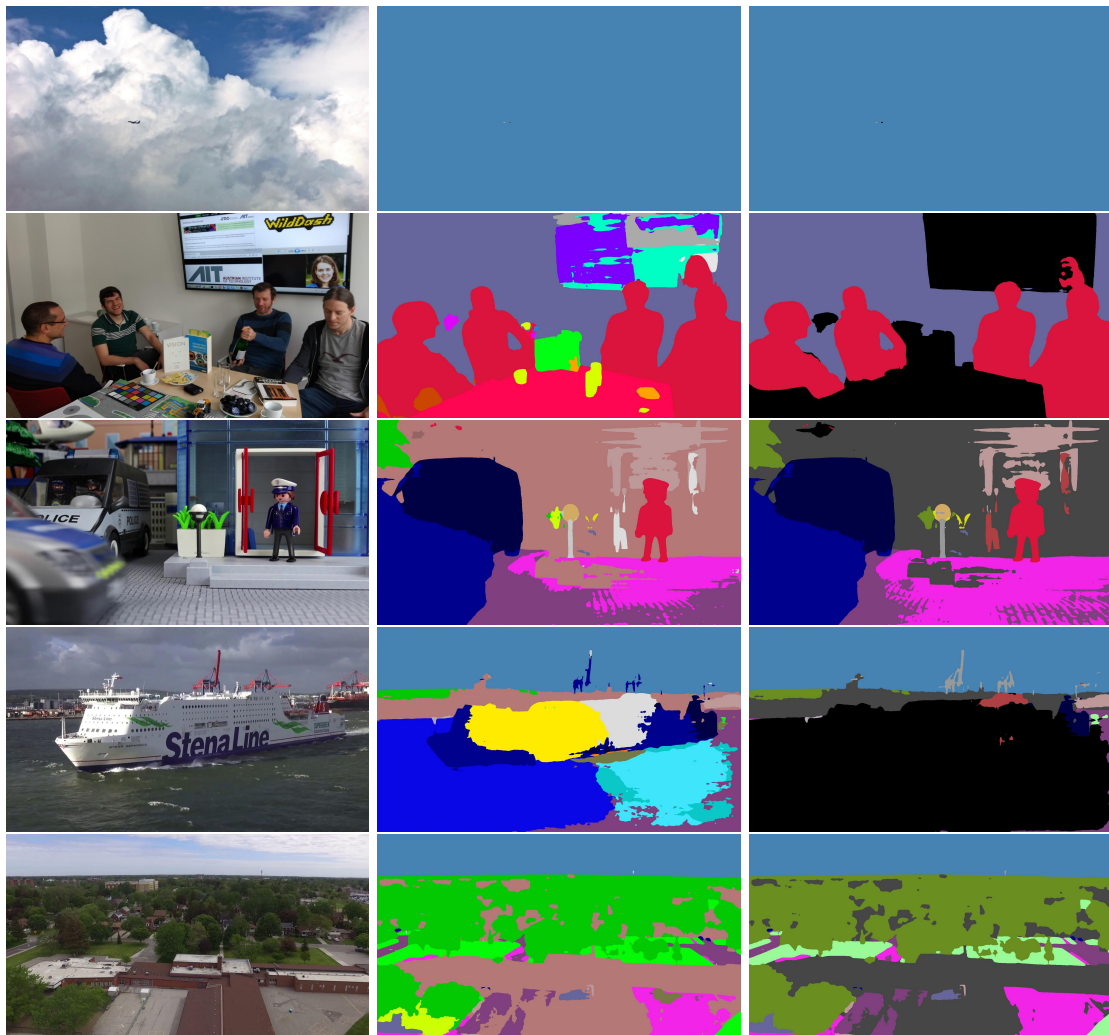


**Fig. 16:** Performance of our universal model UNIV\_CNP\_RVC\_UE on four negative test images from WildDash 2. The columns show the input, universal prediction, and prediction in the WildDash label space where class void is shown in black. Our model successfully recognizes some non-road-driving classes, e.g. table, chair, book, glass and cabinet (row 2), or boat and water (row 4). The model exhibits fair performance in presence of large domain-shift (row 3) and robustness to changed perspective (row 5).

relations. Furthermore, the Mseg taxonomy is limited to the original seven datasets and inflexible to further extensions as it requires pixel-level relabeling. Manual construction of universal taxonomies does require human effort but requires much less time than pixel-level relabeling. Our universal taxonomy for the 10 popular semantic segmentation datasets has been constructed by the first author of this manuscript during less than two days.

We note that multi-dataset training comes with additional challenges (e.g. domain shift) that are not connected to incompatible labelling policies. Multi-dataset training is likely to increase resilience to these issues even though this may not be evident when considering performance on particular datasets that reward overfitting.

## 6 Conclusion

This paper introduces a novel method for training semantic segmentation on a collection of datasets with overlapping classes. We express dataset-specific labels as sets of disjoint universal classes that correspond to distinct visual concepts. Thus, the standard dataset-specific loss can be formulated as negative logarithm of aggregated universal posteriors which we succinctly denote as NLL+. We showcase the flexibility of our approach by implementing it alongside a recent mask-level dense prediction model, where we apply NLL-max loss over universal pixel-assignment masks. In both cases, our approach succeeds to learn universal classes from the original ground-truth in spite of incompatible taxonomies.

Practical implementations of our method require construction of a flat universal taxonomy that spans the desired dataset collection. This calls for recovering a set of disjoint universal classes as well as mapping each dataset-specific class to the corresponding universal counterparts. We propose to solve this problem by considering labels as sets of all possible pixels that should be annotated with the particular label. We hope to encourage future research in the field by publishing the source code [20] for all universal taxonomies from this paper.

Our experiments consider several baselines that map semantically related labels to distinct strongly supervised logits. We show that their performance improves if we consider class relationships during post-inference processing. However,

our method outperforms the baseline performance both in within-dataset and cross-dataset contexts. This suggests that it pays off to resolve semantic incompatibilities before the training. We observe the largest advantage while training on non-biased datasets such as WildDash and Vistas, where implicit dataset detection becomes increasingly difficult and requires considerable capacity. We even show that there are instances where our method can go beyond the semantics of individual datasets by learning a novel concept that does not exist as a distinct class in any of the input taxonomies.

We also compare our approach with the related MSeg taxonomy that supports standard learning with strong supervision on relabeled images. Recall that MSeg taxonomy does not span all classes from the seven involved taxonomies, since it drops 61 fine-grained classes in order to contain the relabeling effort. Empirical comparison on the seven validation splits reveals performance advantage of our universal models. Our models remain competitive even when the evaluation considers only the 194 semantic classes that have been kept or relabeled in the MSeg taxonomy. This suggests that learning on more classes may compensate for weak supervision. Our approach is much more versatile than MSeg since it can be applied to new problems without any relabeling.

To conclude, our work shows that multi-dataset training profits from resolving semantic relationships between individual taxonomies. Our method delivers versatile and robust models that can afford large-scale training on collections of heterogeneous taxonomies. Future work could aim towards advanced evaluation datasets, automatic recovery of universal taxonomies, and applying the proposed framework for open-set recognition.

**Acknowledgments.** This work has been supported by Croatian Science Foundation grant IP-2020-02-5851 ADEPT, by NVIDIA Academic Hardware Grant Program, by European Regional Development Fund grant KK.01.1.1.01.0009 DATACROSS and by VSITE College for Information Technologies who provided access to 6 GPU Tesla-V100 32GB.

**Data Availability Statement.** We perform our experiments on the following publically available datasets: ADE20k [17], BDD [59], Camvid [57], Cityscapes [5], COCO [8], IDD [60], KITTI

[58], MSeg [12], SUN RGBD [61], Scannet [62], Viper [16], Vistas [7], and WildDash 2 [10].

Our universal taxonomy for these datasets is available online [20].

**Published Paper.** This manuscript has been accepted for publication International Journal of Computer Vision, after peer review and is subject to their terms of use, but is not the Version of Record and does not reflect post-acceptance improvements, or any corrections. The Version of Record is available here: <https://www.springerprofessional.de/international-journal-of-computer-vision/11065872>.

## Appendix A Gradients for NLL+ loss

$$\begin{aligned}
 \frac{\partial \mathcal{L}}{\partial s_c} &= \frac{\partial}{\partial s_c} \left( -\ln \sum_{u' \in m_{S_d}(y)} \exp s_{u'} + \ln \sum_u \exp s_u \right) \\
 &= -\mathbb{I}[c \in m_{S_d}(y)] \frac{\exp s_c}{\sum_{u' \in m_{S_d}(y)} \exp s_{u'}} + \frac{\exp s_c}{\sum_u \exp s_u} \\
 &= -\frac{\mathbb{I}[c \in m_{S_d}(y)] \frac{\exp s_c}{\sum_u \exp s_u}}{\sum_{u' \in m_{S_d}(y)} \frac{\exp s_{u'}}{\sum_u \exp s_u}} + \frac{\exp s_c}{\sum_u \exp s_u} \\
 &= -\frac{P(Y = y | U = c) P(U = c | \mathbf{x})}{\sum_{u' \in m_{S_d}(y)} P(U = u' | \mathbf{x})} + P(U = c | \mathbf{x}) \\
 &= -\frac{P(Y = y, U = c | \mathbf{x})}{P(Y = y | \mathbf{x})} + P(U = c | \mathbf{x}) \\
 &= -P(U = c | Y = y, \mathbf{x}) + P(U = c | \mathbf{x}).
 \end{aligned}$$

## References

- [1] Shelhamer E, Long J, Darrell T. Fully Convolutional Networks for Semantic Segmentation. *IEEE Trans Pattern Anal Mach Intell.* 2017;39(4):640–651. <https://doi.org/10.1109/TPAMI.2016.2572683>.
- [2] Rota Bulò S, Porzi L, Kotschieder P. In-place activated batchnorm for memory-optimized training of dnns. In: *Proceedings of the IEEE Conference on Computer Vision and Pattern Recognition*; 2018. p. 5639–5647.
- [3] Oršić M, Šegvić S. Efficient semantic segmentation with pyramidal fusion. *Pattern Recognition.* 2021;p. 107611.
- [4] Cheng B, Misra I, Schwing AG, Kirillov A, Girdhar R. Masked-attention Mask Transformer for Universal Image Segmentation. In: *CVPR*; 2022. p. 1280–1289.
- [5] Cordts M, Omran M, Ramos S, Rehfeld T, Enzweiler M, Benenson R, et al. The cityscapes dataset for semantic urban scene understanding. In: *Proceedings of the IEEE conference on computer vision and pattern recognition*; 2016. p. 3213–3223.
- [6] Everingham M, Gool L, Williams CK, Winn J, Zisserman A. The Pascal Visual Object Classes (VOC) Challenge. *Int J Comp Vis.* 2010;88:303–338.
- [7] Neuhold G, Ollmann T, Rota Bulò S, Kotschieder P. Mapillary Vistas Dataset for Semantic Understanding of Street Scenes. In: *ICCV*; 2017. p. 5000–5009.
- [8] Lin T, Maire M, Belongie SJ, Hays J, Perona P, Ramanan D, et al. Microsoft COCO: Common Objects in Context. In: *ECCV*; 2014. p. 740–755.
- [9] Gupta A, Dollar P, Girshick R. LVIS: A Dataset for Large Vocabulary Instance Segmentation. In: *Proceedings of the IEEE Conference on Computer Vision and Pattern Recognition*; 2019. .
- [10] Zendel O, Honauer K, Murschitz M, Steininger D, Fernandez Dominguez G. WildDash - Creating Hazard-Aware Benchmarks. In: *ECCV*; 2018. .
- [11] Fourure D, Emonet R, Fromont E, Muselet D, Neverova N, Trémeau A, et al. Multi-task, Multi-domain Learning: application to semantic segmentation and pose regression. *Neurocomputing.* 2017;.
- [12] Lambert J, Liu Z, Sener O, Hays J, Koltun V. MSeg: A Composite Dataset for Multi-Domain Semantic Segmentation. In: *CVPR*; 2020. .
- [13] Kim D, Tsai Y, Suh Y, Faraki M, Garg S, Chandraker M, et al. Learning Semantic Segmentation from Multiple Datasets with Label



- Shifts. In: ECCV; 2022. .
- [14] Krešo I, Krapac J, Šegvić S. Efficient ladder-style densenets for semantic segmentation of large images. *IEEE Transactions on Intelligent Transportation Systems*. 2020;.
- [15] Liang X, Zhou H, Xing E. Dynamic-structured semantic propagation network. In: CVPR; 2018. p. 752–761.
- [16] Richter SR, Hayder Z, Koltun V. Playing for Benchmarks. In: ICCV; 2017. p. 2232–2241.
- [17] Zhou B, Zhao H, Puig X, Fidler S, Barriuso A, Torralba A. Scene parsing through ade20k dataset. In: CVPR; 2017. p. 633–641.
- [18] Cour T, Sapp B, Taskar B. Learning from partial labels. *The Journal of Machine Learning Research*. 2011;12:1501–1536.
- [19] Zendel O, Schörghuber M, Rainer B, Murschitz M, Beleznai C. Unifying Panoptic Segmentation for Autonomous Driving. In: Proceedings of the IEEE/CVF Conference on Computer Vision and Pattern Recognition (CVPR); 2022. p. 21351–21360.
- [20] Bevanđić P.: Universal taxonomies for semantic segmentation (source code). Accessed: 2022-12-02. <https://github.com/UNIZG-FER-D307/universal.taxonomies>.
- [21] Orsic M, Bevanđić P, Grubisic I, Saric J, Segvic S. Multi-domain semantic segmentation with pyramidal fusion. arXiv preprint arXiv:200901636, CVPRW RVC. 2020;.
- [22] Bevanđić P, Oršić M, Grubišić I, Šarić J, Šegvić S. Multi-Domain Semantic Segmentation With Overlapping Labels. In: Proceedings of the IEEE/CVF Winter Conference on Applications of Computer Vision (WACV); 2022. p. 2615–2624.
- [23] Bevanđić P, Segvic S. Automatic universal taxonomies for multi-domain semantic segmentation. In: BMVC; 2022. .
- [24] Long J, Shelhamer E, Darrell T. Fully convolutional networks for semantic segmentation. In: Proceedings of the IEEE conference on computer vision and pattern recognition; 2015. p. 3431–3440.
- [25] Chen LC, Papandreou G, Kokkinos I, Murphy K, Yuille AL. Deeplab: Semantic image segmentation with deep convolutional nets, atrous convolution, and fully connected crfs. *IEEE transactions on pattern analysis and machine intelligence*. 2017;40(4):834–848.
- [26] Zhao H, Shi J, Qi X, Wang X, Jia J. Pyramid scene parsing network. In: Proceedings of the IEEE conference on computer vision and pattern recognition; 2017. p. 2881–2890.
- [27] Cheng B, Collins MD, Zhu Y, Liu T, Huang TS, Adam H, et al. Panoptic-deeplab: A simple, strong, and fast baseline for bottom-up panoptic segmentation. In: Proceedings of the IEEE/CVF Conference on Computer Vision and Pattern Recognition; 2020. p. 12475–12485.
- [28] Galleguillos C, Belongie S. Context based object categorization: A critical survey. *Computer Vision and Image Understanding*. 2010 06;114:712–722. <https://doi.org/10.1016/j.cviu.2010.02.004>.
- [29] Schwartz R, Dodge J, Smith NA, Etzioni O. Green AI. *Commun ACM*. 2020;63(12):54–63.
- [30] Zhao H, Qi X, Shen X, Shi J, Jia J. ICNet for Real-Time Semantic Segmentation on High-Resolution Images. In: Ferrari V, Hebert M, Sminchisescu C, Weiss Y, editors. *Computer Vision - ECCV 2018 - 15th European Conference, Munich, Germany, September 8-14, 2018, Proceedings, Part III*. vol. 11207 of *Lecture Notes in Computer Science*. Springer; 2018. p. 418–434.
- [31] Yu F, Koltun V. Multi-Scale Context Aggregation by Dilated Convolutions. In: *International Conference on Learning Representations (ICLR)*; 2016. .

- [32] Sandler M, Howard A, Zhu M, Zhmoginov A, Chen LC. MobileNetV2: Inverted Residuals and Linear Bottlenecks; 2018. p. 4510–4520.
- [33] Ronneberger O, Fischer P, Brox T. U-net: Convolutional networks for biomedical image segmentation. In: International Conference on Medical image computing and computer-assisted intervention. Springer; 2015. p. 234–241.
- [34] Zhou T, Wang W, Konukoglu E, Van Goo L. Rethinking Semantic Segmentation: A Prototype View. In: CVPR; 2022. p. 2572–2583.
- [35] Cheng B, Schwing AG, Kirillov A. Per-Pixel Classification is Not All You Need for Semantic Segmentation. In: NeurIPS; 2021. .
- [36] Cheng B, Misra I, Schwing AG, Kirillov A, Girdhar R. Masked-attention Mask Transformer for Universal Image Segmentation. In: CVPR; 2022. .
- [37] Li L, Zhou T, Wang W, Li J, Yang Y. Deep Hierarchical Semantic Segmentation. In: 2022 IEEE/CVF Conference on Computer Vision and Pattern Recognition (CVPR); 2022. p. 1236–1247.
- [38] Sun C, Shrivastava A, Singh S, Gupta A. Revisiting Unreasonable Effectiveness of Data in Deep Learning Era. In: IEEE International Conference on Computer Vision, ICCV 2017, Venice, Italy, October 22-29, 2017. IEEE Computer Society; 2017. p. 843–852.
- [39] Zlateski A, Jaroensri R, Sharma P, Durand F. On the Importance of Label Quality for Semantic Segmentation. In: CVPR; 2018. p. 1479–1487.
- [40] : Robust Vision Challenge. Accessed: 2022-12-02. <http://www.robustvision.net/index.php>.
- [41] Chan R, Rottmann M, Gottschalk H. Entropy Maximization and Meta Classification for Out-of-Distribution Detection in Semantic Segmentation. In: International Conference on Computer Vision, ICCV; 2021.
- [42] Biase GD, Blum H, Siegwart R, Cadena C. Pixel-Wise Anomaly Detection in Complex Driving Scenes. In: Computer Vision and Pattern Recognition, CVPR; 2021. .
- [43] Bevandić P, Krešo I, Oršić M, Šegvić S. Dense open-set recognition based on training with noisy negative images. Image and Vision Computing. 2022;124:104490. <https://doi.org/https://doi.org/10.1016/j.imavis.2022.104490>.
- [44] Kalluri T, Varma G, Chandraker M, Jawahar C. Universal semi-supervised semantic segmentation. In: Proceedings of the IEEE International Conference on Computer Vision; 2019. p. 5259–5270.
- [45] Masaki S, Hirakawa T, Yamashita T, Fujiyoshi H. Multi-Domain Semantic-Segmentation using Multi-Head Model. In: 2021 IEEE International Intelligent Transportation Systems Conference (ITSC); 2021. p. 2802–2807.
- [46] Zhou X, Koltun V, Krähenbühl P. Simple multi-dataset detection. In: CVPR; 2022. .
- [47] Meletis P, Dubbelman G. Training of Convolutional Networks on Multiple Heterogeneous Datasets for Street Scene Semantic Segmentation. In: Intelligent Vehicles Symposium; 2018. p. 1045–1050.
- [48] Zhao X, Schuster S, Sharma G, Tsai Y, Chandraker M, Wu Y. Object Detection with a Unified Label Space from Multiple Datasets. In: ECCV; 2020. p. 178–193.
- [49] Zhu Y, Sapra K, Reda FA, Shih KJ, Newsam S, Tao A, et al. Improving semantic segmentation via video propagation and label relaxation. In: Proceedings of the IEEE Conference on Computer Vision and Pattern Recognition; 2019. p. 8856–8865.
- [50] McClosky D, Charniak E, Johnson M. Effective Self-Training for Parsing. In: NAACL; 2006. p. 152–159.

- [51] Lee DH. Pseudo-Label : The Simple and Efficient Semi-Supervised Learning Method for Deep Neural Networks. WREPL. 2013 07;.
- [52] Yin W, Liu Y, Shen C, van den Hengel A, Sun B. The devil is in the labels: Semantic segmentation from sentences. CoRR. 2022;abs/2202.02002.
- [53] Uijlings JRR, Mensink T, Ferrari V. The Missing Link: Finding Label Relations Across Datasets. In: ECCV; 2022. p. 540–556.
- [54] He K, Zhang X, Ren S, Sun J. Deep residual learning for image recognition. In: Proceedings of the IEEE conference on computer vision and pattern recognition; 2016. p. 770–778.
- [55] Huang G, Liu Z, Pleiss G, Van Der Maaten L, Weinberger K. Convolutional networks with dense connectivity. IEEE transactions on pattern analysis and machine intelligence. 2019;.
- [56] Zhen M, Wang J, Zhou L, Fang T, Quan L. Learning Fully Dense Neural Networks for Image Semantic Segmentation. In: AAAI; 2019. .
- [57] Badrinarayanan V, Kendall A, Cipolla R. SegNet: A Deep Convolutional Encoder-Decoder Architecture for Image Segmentation. IEEE Trans Pattern Anal Mach Intell. 2017;39(12):2481–2495.
- [58] Geiger A, Lenz P, Stiller C, Urtasun R. Vision meets robotics: The KITTI dataset. Int J Robotics Res. 2013;32(11):1231–1237.
- [59] Yu F, Xian W, Chen Y, Liu F, Liao M, Madhavan V, et al. BDD100K: A Diverse Driving Video Database with Scalable Annotation Tooling. arXiv preprint arXiv:180504687. 2018;.
- [60] Varma G, Subramanian A, Namboodiri AM, Chandraker M, Jawahar CV. IDD: A Dataset for Exploring Problems of Autonomous Navigation in Unconstrained Environments. In: WACV; 2019. p. 1743–1751.
- [61] Song S, Lichtenberg SP, Xiao J. SUN RGB-D: A RGB-D scene understanding benchmark suite. In: CVPR; 2015. p. 567–576.
- [62] Dai A, Chang AX, Savva M, Halber M, Funkhouser T, Nießner M. ScanNet: Richly-annotated 3D Reconstructions of Indoor Scenes. In: CVPR; 2017. .
- [63] Kreso I, Krapac J, Segvic S. Efficient Ladder-Style DenseNets for Semantic Segmentation of Large Images. IEEE Trans Intell Transp Syst. 2021;22(8):4951–4961.
- [64] Mohan R, Valada A. EfficientPS: Efficient Panoptic Segmentation. International Journal of Computer Vision. 2020;129:1551 – 1579.
- [65] Porzi L, Bulò SR, Colovic A, Kotschieder P. Seamless Scene Segmentation. In: CVPR; 2019. p. 8277–8286.
- [66] Kim D, Tsai Y, Suh Y, Faraki M, Garg S, Chandraker M, et al. Learning Semantic Segmentation from Multiple Datasets with Label Shifts. CoRR. 2022;abs/2202.14030.
- [67] Xiao J, Xu Z, Lan S, Yu Z, Yuille A, Anandkumar A. 1st Place Solution of The Robust Vision Challenge 2022 Semantic Segmentation Track. CoRR. 2022;abs/2210.12852.
- [68] Liu Y, Ge P, Liu Q, Fan S, Wang Y. An Empirical Study on Multi-Domain Robust Semantic Segmentation. arXiv preprint arXiv:221204221. 2022;.
- [69] Chan R, Lis K, Uhlemeyer S, Blum H, Honari S, Siegwart R, et al. SegmentMeIfYouCan: A Benchmark for Anomaly Segmentation. In: Vanschoren J, Yeung S, editors. NeurIPS; 2021. .
- [70] Blum H, Sarlin P, Nieto JI, Siegwart R, Cadena C. The Fishyscapes Benchmark: Measuring Blind Spots in Semantic Segmentation. Int J Comput Vis. 2021;129(11):3119–3135.